Squeezed momentum distributions of relativistic electrons in intense laser fields with arbitrary polarization

C. H. Raymond Ooi,[1] Szczepan Chelkowski,[2] and Andre D. Bandrauk[2]
[1]*Department of Physics, University of Malaya, 50603 Kuala Lumpur, Malaysia*
[2]*Laboratoire de Chimie Théorique, Faculté des Sciences, Université de Sherbrooke, Sherbrooke, Québec, Canada J1K 2R1*

(Received 21 June 2019; revised manuscript received 14 October 2019; published 3 January 2020)

We investigate the dynamics of relativistic electrons interacting with intense laser fields in a linear or circular polarization. First, we study the momentum distributions of a single spatially localized wave packet. We find that these distributions are squeezed in the polarization plane (y-z) as well as along the laser propagation (x) direction. In a chosen gauge, the squeezing direction is controlled by the laser vector potential **A** and the electron initial momentum. For the case when the electron initial momentum is zero the squeezing occurs directly along the direction of **A**. We obtain analytical expressions within linear momentum approximation that explain the squeezing features very well by defining a squeezing vector and rotational angle of the squeezed momentum distribution. We analyze the symmetric properties of the momentum distributions viewed in different momentum planes and discuss the effects of different helicity of circular laser polarizations and the direction of the spin quantization. An unexpected feature of bending of momentum distribution is found for very intense laser fields. We extend our investigation to the momentum distribution of two spatially separated wave packets, particularly the orientations of two crossing distributions. It is found that the absolute phase of the initial laser field affects the orientation of the electron momentum distributions while quantum superposition of two states with the same spin gives interference in the momentum distributions that depends on the quantum phase of the electron.

DOI: 10.1103/PhysRevA.101.013401

I. INTRODUCTION

In connection with recent extraordinary development of high power laser sources much effort has been devoted to the theory of interaction of intense radiation with matter. At currently available lasers exceeding intensities 10^{18} W/cm^2 [1,2] relativistic description based on the Dirac equation is necessary. This is a theoretical challenge since no analytic solutions are known for the Dirac equation describing the dynamics of an atomic (bound) electron interacting with an intense laser field. Most theoretical work is based on the premise that at high fields the solution of the Dirac equation is known for an unbound electron interacting with an electromagnetic classical plane wave (called the Volkov solution). This solution was found long ago, in 1935, by Volkov [3]. Its derivation can also be found in the textbook [4] and in a recent review [5]. This exact analytical solution appeared to be very useful in the description of various phenomena, particularly in description of photoionization of atoms in the framework of the so-called strong-field approximation, the approach developed by the pioneering work of Reiss [6,7]. In this framework the Volkov solution is incorporated in the transition amplitude and the approximation consists in treating electron-nucleus interaction as perturbation. In the nonrelativistic limit [8] and within the dipole approximation one can derive an important nonrelativistic long-wavelength limit called the Keldysh tunneling theory of photoionization [9]. As shown by Reiss and Krainov [10] and later by Bauer [11], the nonrelativistic Volkov solution can be used to obtain analytical solutions for the electron wave function in the atomic Coulomb potential interacting with a strong circularly polarized laser field.

The Volkov wave function has also been applied in various other phenomena such as scattering problems [12,13], nonlinear Compton scattering (see [14] and references therein), and also quantum dynamics of free electrons in problems involving electron-spin dynamics in a quantized laser field [15]. Recent works also generalize the Volkov solutions to a medium with refractive index [16] and inclusion of photon effective mass in plasma [17], which involves solving second-order differential equations and incorporating the WKB approach to strong-field QED [1]. The Volkov solution will also be useful in connection with recent investigations of the problem of the transfer of photon momentum from a laser into an electron and nucleus in intense laser fields (see [18] and references therein).

We note that the original Volkov wave function used in most of the above-mentioned applications corresponds to plane-wave-like electron states. In order to describe a localized electron it is necessary to construct a suitable superposition of Volkov states each labeled by the momentum vector **p** with amplitudes $c(\mathbf{p})$ inside the superposition. Several authors studied this problem recently. Two different approaches have been used. In the first approach [19,20] one assumes *ad hoc* the shape of these amplitudes $c(\mathbf{p})$ (assumed as Gaussians) where in another approach [21] one assumes a known spatial shape of the wave packet at some specific (initial) time when the electromagnetic field is nonzero. In the latter approach the amplitudes $c(\mathbf{p})$ should be calculated by projecting the known spatial shape on the Volkov wave functions. In this

paper we follow the latter approach described in detail in [21] where the amplitudes are computed numerically and used to study the evolution in configuration space at later times. In our paper we investigate in detail the surprising squeezed shapes of momentum distributions described by $|c(\mathbf{p})|^2$ which were not discussed in [21]. In nonrelativistic laser electron dynamics (based on the dipole approximation) a simple Gaussian spatial wave packet corresponds to simple Gaussian momentum amplitudes $c(\mathbf{p})$. However, we find that in the relativistic case the simple Gaussian spatial wave packet is built with more complex (squeezed and rotated) momentum amplitudes $c(\mathbf{p})$.

Next we investigate the relativistic phenomena of quantum superpositions of two wave packets, i.e., superposition of two states of an electron (namely, different spin and spatially separated center of wave-packet degrees of freedom) on the momentum distributions under linearly, circularly, or elliptically polarized intense laser fields. In practice, a relativistic electron generated in a particle accelerator can travel in two opposite directions. The setup can be achieved by passing the electron through a double slit (depicted in Fig. 1) where the electron is spin flipped if passing through the lower slit and its direction can be controlled by the presence or absence of the mirror.

The laser-electron system is described by the covariant Dirac equation which includes not only relativistic speed [22] but also the spin property of the electron, as given in Sec. II. Full analytical solutions of the time-dependent wave functions are obtained for an initial Gaussian spatial wave packet in Sec III. Results of three-dimensional (3D) plots in momentum space are obtained. In Sec IV, we analyze the momentum distributions of the relativistic electron states and see how they are affected by the laser parameters such as field strength, polarization, and spatial-temporal dependence of the laser phase. This paper provides insights on the effects of intense fields on the quantum superposition properties of the electron.

II. INTERACTION OF ELECTROMAGNETIC FIELDS WITH A RELATIVISTIC ELECTRON

In the presence of EM fields interacting with a spin particle, the Dirac equation is [4]

$$(\not{p} - e\not{A} - mc)\psi^s = 0 \tag{1}$$

with $\not{A} = \gamma^\mu A_\mu$, $\not{p} = \gamma^\mu p_\mu = \gamma^\mu i\hbar\partial_\mu$, and the four-component spinor ψ^s as the solutions, with the matrix written as

$$\gamma = \begin{pmatrix} \mathbf{0} & \hat{\sigma} \\ -\hat{\sigma} & \mathbf{0} \end{pmatrix}, \tag{2}$$

where $\hat{\boldsymbol{\sigma}}$ represents the usual three 2×2 Pauli matrices. The derivation of the Volkov equation as the solution of the Dirac equation is given in Appendix A.

General elliptically polarized laser

The Dirac equation is solved in Appendix A, giving the final Volkov wave function (for any plane-wave laser, not necessarily monochromatic) [21]

$$\psi^{\pm}(\mathbf{p};\mathbf{r},t) = N(E)\left(1 \pm \frac{e\not{k}\not{A}}{2k\cdot p}\right)u^{\pm}(\mathbf{p})e^{iS^{\pm}} \tag{3}$$

where the action phase is

$$S^{\pm} = \mp\frac{p\cdot x}{\hbar} + \int_{-\infty}^{k\cdot x}\left[-\frac{eA\cdot p}{\hbar(k\cdot p)} \pm \frac{e^2A^2}{2\hbar(k\cdot p)}\right]d\varphi \tag{4}$$

with $k\cdot p = \frac{\omega}{c}\frac{E}{c} - k_x p_x, A\cdot p = \frac{\phi}{c}\frac{E}{c} - \mathbf{A}\cdot\mathbf{p} = -A_y p_y - A_z p_z$, and $A^2 = (\frac{\phi}{c})^2 - |\mathbf{A}|^2$. The upper (lower) sign is for positive (negative) energy.

We assume the laser beam propagates along the x direction $\mathbf{k} = k_x\hat{x}$ as a monochromatic plane wave with a general

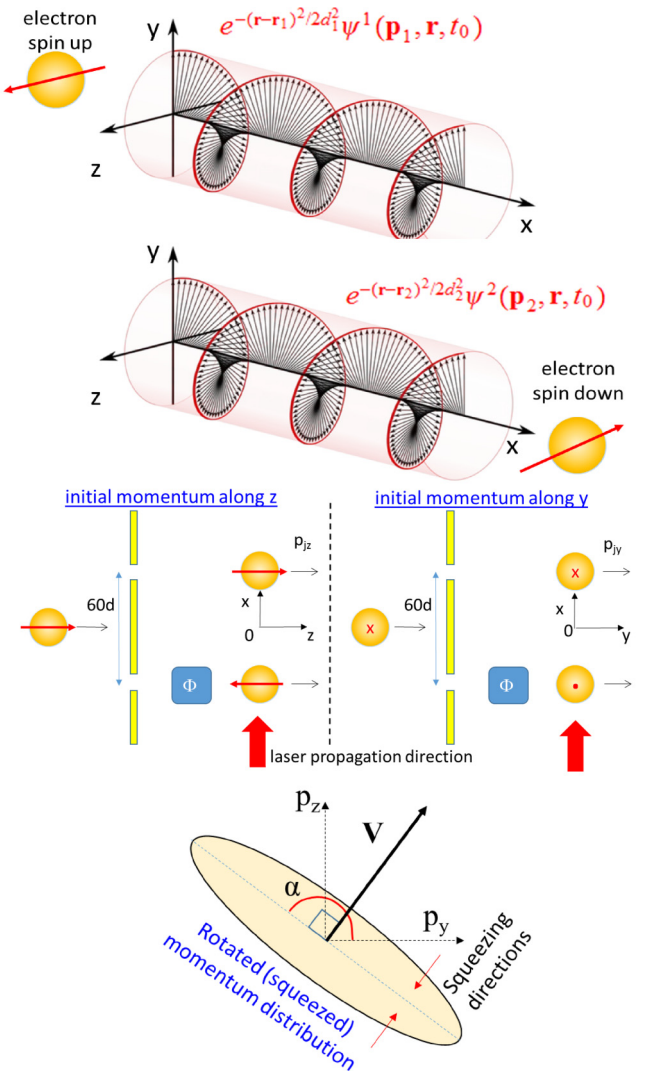

FIG. 1. Schematic of a generally elliptically polarized laser field interacting with an electron initially in the superposition of spin up and spin down for chosen initial positions and quasimomenta of which are our choice. The picture in the middle shows how the superposition state can be created by a double slit setup with spin flip and a Φ phase control apparatus. The bottom picture shows the squeezing vector **V** defined in Eq. (55) and the rotational angle α of the squeezed momentum distribution in the y-z plane, perpendicular to the x direction.

elliptically polarized vector potential

$$\mathbf{A}(\varphi) = a_y\hat{y}\cos\varphi + a_z\hat{z}\cos(\varphi+\delta) \tag{5}$$

which satisfies the transversality condition $\mathbf{k}\cdot\mathbf{A} = \mathbf{0}$, where $\varphi = \omega t - k_x x$.

The bracket matrix in Eq. (3) takes the form

$$\begin{pmatrix} 1\mp iY\epsilon & \pm Z\epsilon & \mp Z & \pm iY \\ \mp Z\epsilon & 1\pm iY\epsilon & \mp iY & \pm Z \\ \mp Z & \pm iY & 1\mp iY\epsilon & \pm Z\epsilon \\ \mp iY & \pm Z & \mp Z\epsilon & 1\pm iY\epsilon \end{pmatrix} \tag{6}$$

with $Y=\frac{k_0 eA_y(\varphi)}{2k\cdot p}$, $Z=\frac{k_0 eA_z(\varphi)}{2k\cdot p}$, $A_y=a_y\cos\varphi$, $A_z = a_z\cos(\varphi+\delta)$, $\epsilon = \frac{k_x}{k_0}$, and $k_0 = \frac{\omega}{c}$. We have assumed the Coulomb gauge with scalar potential $\phi = 0$, hence the electric field is $\mathbf{E} = -\frac{\partial\mathbf{A}}{\partial t}$, antiparallel to $\mathbf{A}$. Note that the amplitude of the Volkov solution acquires significant time dependence through φ at high field as the magnitude of $\frac{k_0 ea_{y,z}}{2k\cdot p}$ can become comparable to or greater than unity.

Putting in the zero-field solutions $u^{\pm}$ we have the four solutions

$$\psi^1 = N\begin{pmatrix} 1+iY(P_+-\epsilon)-ZP_z \\ -iYP_z + Z(P_+-\epsilon) \\ P_z(1-iY\epsilon)+Z(\epsilon P_+-1) \\ P_+ + iY(\epsilon P_+-1) - Z\epsilon P_z \end{pmatrix} e^{iS^+}, \tag{7}$$

$$\psi^2 = N\begin{pmatrix} -iYP_z + Z(\epsilon-P_-) \\ 1+iY(\epsilon-P_-)-ZP_z \\ P_- + iY(1-\epsilon P_-) - Z\epsilon P_z \\ -P_z - iY\epsilon P_z + Z(1-\epsilon P_-) \end{pmatrix} e^{iS^+}, \tag{8}$$

$$\psi^3 = N\begin{pmatrix} P_z + iY\epsilon P_z + Z(1-\epsilon P_+) \\ P_+ + iY(1-\epsilon P_+) + Z\epsilon P_z \\ 1+iY(\epsilon-P_+)+ZP_z \\ iYP_z + Z(\epsilon-P_+) \end{pmatrix} e^{iS^-}, \tag{9}$$

$$\psi^4 = N\begin{pmatrix} P_- + iY(\epsilon P_- - 1) + Z\epsilon P_z \\ -P_z + iY\epsilon P_z + Z(\epsilon P_- - 1) \\ iYP_z + Z(P_- - \epsilon) \\ 1+iY(P_- - \epsilon) + ZP_z \end{pmatrix} e^{iS^-} \tag{10}$$

where $P_j = \frac{cp_j}{E+mc^2}$, $j = z, \pm$.

III. PROBABILITIES IN MOMENTUM SPACE

The spatial-temporal dynamics of the relativistic electron is described by superpositions of wave functions $\psi^s(\mathbf{p};\mathbf{r},t)$ of the four solutions of the Dirac equation; each is a four-component spinor, containing amplitudes and phases of electron spin up ($s = 1$), electron spin down ($s = 2$), positron spin up ($s = 3$), and positron spin down ($s = 4$):

$$\Psi(\mathbf{r},t) = \int d^3p \sum_{s=1}^{4} c^s(\mathbf{p})\psi^s(\mathbf{p};\mathbf{r},t). \tag{11}$$

Consider that the initial state of the electron is a superposition of spin up and spin down, each with a central momentum $\mathbf{p}_j$ and central position $\mathbf{r}_j$ described by a Gaussian-type wave packet, and $e^{-(\mathbf{r}-\mathbf{r}_j)^2/2d_j^2}$ is introduced into the cw laser field at a specific time, such that $\theta_j = \omega t_0 - k_x x_j$, corresponding to laser vector potential $\mathbf{A} = \frac{a}{\sqrt{2}}(\hat{y}+\hat{z})\cos\theta_j$ for linear polarization (when $\delta = 0$) and $\mathbf{A} = \frac{a}{\sqrt{2}}(\hat{y}\cos\theta_j - \hat{z}\sin\theta_j)$ for circular polarization (when $\delta = \pm\pi/2$):

$$\Psi(\mathbf{r},t_0) = N_0\big[e^{i\Phi_1}e^{-(\mathbf{r}-\mathbf{r}_1)^2/2d_1^2}\psi^1(\mathbf{p}_1;\mathbf{r},t_0) + e^{i\Phi_2}e^{-(\mathbf{r}-\mathbf{r}_2)^2/2d_2^2}\psi^2(\mathbf{p}_2;\mathbf{r},t_0)\big] \tag{12}$$

where the normalization parameter for the given initial condition is $N_0^2\sum_{j=1}^{2}\int e^{-(\mathbf{r}-\mathbf{r}_j)^2/d_j^2}|\psi^j(\mathbf{p}_j;\mathbf{r},t_0)|^2 d^3r = 1$.

In practice the phase difference $\Phi = \Phi_1 - \Phi_2$ may be controlled to give the desired interference effect. We also notice that the time-averaged intensity ($|\mathbf{A}|^2$ integrated over one cycle) is the same for both linear and circular polarizations.

The initial states (for electron spin up and spin down) are, respectively,

$$\psi^1(\mathbf{p}_1;\mathbf{r},t_0) = N_1\begin{pmatrix} iY_1(P_{1+}-\epsilon)-Z_1P_{1z}+1 \\ Z_1(P_{1+}-\epsilon)-iY_1P_{1z} \\ P_{1z}(1-iY_1\epsilon)+Z_1(\epsilon P_{1+}-1) \\ P_{1+}-Z_1\epsilon P_{1z}+iY_1(\epsilon P_{1+}-1) \end{pmatrix} e^{iS^+(\mathbf{p}_1,\varphi_0)}, \tag{13}$$

$$\psi^2(\mathbf{p}_2;\mathbf{r},t_0) = N_2\begin{pmatrix} -iY_2P_{2z}+Z_2(\epsilon-P_{2-}) \\ 1+iY_2(\epsilon-P_{2-})-Z_2P_{2z} \\ P_{2-}+iY_2(1-\epsilon P_{2-})-Z_2\epsilon P_{2z} \\ -P_{2z}-iY_2\epsilon P_{2z}+Z_2(1-\epsilon P_{2-}) \end{pmatrix} e^{iS^+(\mathbf{p}_2,\varphi_0)} \tag{14}$$

where $Y_j = \frac{k_0 ea_y}{2k\cdot p_j}\cos\varphi_0$, $Z_j = \frac{k_0 ea_z}{2k\cdot p_j}\cos(\varphi_0+\delta)$, $\varphi_0 = k\cdot x_0 = \omega t_0 - k_x x$, $N_j = \sqrt{\frac{E_j+mc^2}{(2\pi)^3 2E_j}}$, and

$$S^+(\mathbf{p}_j,\varphi_0) = \frac{\mathbf{p}_j\cdot\mathbf{r}-E_jt_0}{\hbar} + \frac{1}{\hbar k\cdot p_j}\Big[ep_{jy}a_y\sin\varphi_0 + ep_{jz}a_z\sin(\varphi_0+\delta) + \Big(\frac{ea_y}{2}\Big)^2 g(\varphi_0) + \Big(\frac{ea_z}{2}\Big)^2 g(\varphi_0+\delta)\Big] \tag{15}$$

where $g(u) = u + \frac{1}{2}\sin 2u$.

To compute the coefficient $c^s(\mathbf{p}')$, the probability amplitude for finding the system in any time in the Volkov state $\psi^s(\mathbf{p}';\mathbf{r},t)$, following San Roman *et al.* [21], we take the projection of the known initial wave function $\Psi(\mathbf{r},t_0)$ in Eqs. (11) and (12) at time t_0 on $\psi^s(\mathbf{p}';\mathbf{r},t_0)$, which is the scalar product

$$c^s(\mathbf{p}) = \int d^3r\psi^{s*}(\mathbf{p};\mathbf{r},t_0)\Psi(\mathbf{r},t_0) \tag{16}$$

$$= N_0\sum_{j=1}^{2} e^{i\Phi_j}\int d^3r e^{-(\mathbf{r}-\mathbf{r}_j)^2/2d_j^2}\psi^{s*}(\mathbf{p};\mathbf{r},t_0)\psi^j(\mathbf{p}_j;\mathbf{r},t_0) \tag{17}$$

where we use the orthonormality $\int d^3r\psi^{r*}(\mathbf{p}';\mathbf{r},t)\,\psi^s(\mathbf{p};\mathbf{r},t) = \delta(\mathbf{p}'-\mathbf{p})\delta_{sr}$ or $\langle\psi^s(\mathbf{p};\mathbf{r},t)|\psi^r(\mathbf{p};\mathbf{r},t)\rangle = \delta_{sr}$. The normalization of the wave function $\Psi(\mathbf{r},t) = \sum_{s=1\ldots4}\Psi^s(\mathbf{r},t)$ gives $\int d^3r|\Psi^s(\mathbf{r},t)|^2 = \int d^3p|c^s(\mathbf{p})|^2$ and $N_0 \sim (\frac{2\pi}{d\sqrt{\pi}})^{3/2}$.

Here Y is replaced by $Y_0 = \frac{k_0 e a_y}{2k\cdot p}\cos\varphi_0$ and Z is replaced by $Z_0 = \frac{k_0 e a_z}{2k\cdot p}\cos(\varphi_0+\delta)$. The phase of $\psi^s(\mathbf{p};\mathbf{r},t_0)$ in Eqs. (7)–(10) depends on t_0, which determines the *initial condition* (such as position, momentum of the electron, and the field experienced). Thus, according to Eq. (16) $c^s(\mathbf{p})$ does not change with time and is fixed by the initial condition.

Four different paired products need to be calculated; a general paired product is expressed as

$$\psi^{s*}(\mathbf{p};\mathbf{r},t_0)\psi^j(\mathbf{p}_j;\mathbf{r},t_0) = \frac{1}{(2\pi)^3}\sqrt{\frac{E+mc^2}{2E}}\sqrt{\frac{E_j+mc^2}{2E_j}}u^{s\dagger}(\mathbf{p};\mathbf{r},t_0)u^j(\mathbf{p}_j;\mathbf{r},t_0)e^{i[-S^{\pm}(\mathbf{p};\varphi_0)+S^{+}(\mathbf{p}_j;\varphi_0)]}, \tag{18}$$

$$S^{\pm}(\mathbf{p};\varphi_0) = \mp\frac{Et_0-\mathbf{p}\cdot\mathbf{r}}{\hbar} + \frac{1}{\hbar k\cdot p}\left[ep_y a_y\sin\varphi_0 + ep_z a_z\sin(\varphi_0+\delta) \pm \left(\frac{ea_y}{2}\right)^2 g(\varphi_0) \pm \left(\frac{ea_z}{2}\right)^2 g(\varphi_0+\delta)\right]. \tag{19}$$

The general argument has the form

$$u^{s\dagger}(\mathbf{p};\mathbf{r},t_0)u^j(\mathbf{p}_j,\mathbf{r},t_0) = f_1 + \sum_{d=0,\delta}\{f_{2d}\cos(\varphi_0+d) + f_{3d}\cos^2(\varphi_0+d)\} + f_{23}\cos\varphi_0\cos(\varphi_0+\delta) \tag{20}$$

and the exponential

$$\begin{aligned} -S^{\pm}(\mathbf{p};\varphi_0) + S^{+}(\mathbf{p}_j,\varphi_0) &= \frac{(\pm p - p_j)\cdot x_0}{\hbar} + \frac{1}{\hbar}\int_{-\infty}^{k\cdot x_0} e\left[\frac{p}{k\cdot p} - \frac{p_j}{k\cdot p_j}\right]\cdot A(\varphi')d\varphi' \\ &\quad + \frac{1}{\hbar}\int_{-\infty}^{k\cdot x_0}\left[\frac{1}{(k\cdot p_j)} \mp \frac{1}{(k\cdot p)}\right]\frac{1}{2}e^2A(\varphi')^2 d\varphi' \qquad (21) \\ &= \varphi_j^{\mp} + \mathbf{f}_{4j}^{\mp}\cdot\mathbf{r} + \sum_{d=0,\delta}\{f_{5jd}\sin(\varphi_0+d) + f_{6jd}^{\mp}\sin 2(\varphi_0+d)\} \qquad (22) \end{aligned}$$

where

$$\hbar\varphi_j^{\mp} = \left\{(-\mp E - E_j) + W_{j\mp}\left[\left(\frac{ea_y}{2}\right)^2 + \left(\frac{ea_z}{2}\right)^2\right]\omega\right\}t_0 + W_{j\mp}\left(\frac{ea_z}{2}\right)^2\delta, \tag{23}$$

$$\hbar\mathbf{f}_{4j}^{\mp} = (\mp\mathbf{p}+\mathbf{p}_j) - \mathbf{k}W_{j\mp}\left[\left(\frac{ea_y}{2}\right)^2 + \left(\frac{ea_z}{2}\right)^2\right], \tag{24}$$

$$\hbar f_{5j} = -e\Delta_{jy}a_y,\ \hbar f_{5j\delta} = -e\Delta_{jz}a_z, \tag{25}$$

$$\hbar f_{6j}^{\mp} = W_{j\mp}\left(\frac{ea_y}{2}\right)^2\frac{1}{2},\ \hbar f_{6j\delta}^{\mp} = W_{j\mp}\left(\frac{ea_z}{2}\right)^2\frac{1}{2}, \tag{26}$$

with $\Delta_{jy} = \frac{p_y}{k\cdot p} - \frac{p_{jy}}{k\cdot p_j}$, $\Delta_{jz} = \frac{p_z}{k\cdot p} - \frac{p_{jz}}{k\cdot p_j}$, $W_{j\mp} = \frac{1}{k\cdot p_j} \mp \frac{1}{k\cdot p}$, and $a^2 = a_y^2 + a_z^2$.

The f coefficients all depend on the indices s and j. For example, for $s=1$ and $j=1$

$$u^{1\dagger}(\mathbf{p};\mathbf{r},t_0) = \begin{pmatrix} -iY_0(P_- - \epsilon) - Z_0P_z + 1 \\ Z_0(P_- - \epsilon) + iY_0P_z \\ P_z + iY_0\epsilon P_z + Z_0(\epsilon P_- - 1) \\ P_- - Z_0\epsilon P_z - iY_0(\epsilon P_- - 1)\end{pmatrix}^T, \tag{27}$$

$$u^{1}(\mathbf{p}_1,\mathbf{r},t_0) = \begin{pmatrix} iY_1(P_{1+} - \epsilon) - Z_1P_{1z} + 1 \\ Z_1(P_{1+} - \epsilon) - iY_1P_{1z} \\ P_{1z} - iY_1\epsilon P_{1z} + Z_1(\epsilon P_{1+} - 1) \\ P_{1+} - Z_1\epsilon P_{1z} + iY_1(\epsilon P_{1+} - 1)\end{pmatrix}. \tag{28}$$

The coefficients can be written in the general form

$$\begin{aligned} c^s(\mathbf{p}) &= \frac{N_0}{(2\pi)^3}\sqrt{\frac{E+mc^2}{2E}}\sum_{j=1}^{2}\sqrt{\frac{E_j+mc^2}{2E_j}}e^{i\Phi_j}e^{i\varphi_j^{\mp}}e^{i(f_{4jy}^{\mp}y_j + f_{4jz}^{\mp}z_j)}e^{-f_{4jy}^{\mp\,2}d_j^2/2}e^{-f_{4jz}^{\mp\,2}d_j^2/2}\left(2\pi d_j^2\right) \\ &\quad\times\int_{-\infty}^{\infty}e^{-(x-x_j)^2/2d_j^2}u^{s\dagger}(\mathbf{p};\mathbf{r},t_0)u^j(\mathbf{p}_j,\mathbf{r},t_0)e^{if_{4jx}^{\mp}x + i\sum\limits_{d=0,\delta}\{f_{5jd}\sin(\varphi_0+d) + f_{6jd}^{\mp}\sin 2(\varphi_0+d)\}}dx \end{aligned} \tag{29}$$

where the superscript "$-(+)$" corresponds to $s=1,2,(3,4)$ and we have used

$$\int_{-\infty}^{\infty}e^{-(z-z_j)^2/2d_j^2}e^{if_{4jz}^{\mp}z}dz = e^{if_{4jz}z_j}\int_{-\infty}^{\infty}e^{-z'^2/2d_j^2}e^{if_{4jz}^{\mp}z'}dz' = e^{if_{4jz}^{\mp}z_j}e^{-f_{4jz}^{\mp\,2}d_j^2/2}\left(2\pi d_j^2\right)^{1/2}. \tag{30}$$

The coefficients can be evaluated analytically as (only for the cw laser field)

$$c^s(\mathbf{p}) = \frac{N_0}{(2\pi)^3}\sqrt{\frac{E+mc^2}{2E}}\sum_{j=1}^{2} e^{i\Phi_j}\sqrt{\frac{E_j+mc^2}{2E_j}}e^{i\varphi_j^{\mp}}e^{-f_{4jy}{}^2d_j^2/2}e^{-f_{4jz}{}^2d_j^2/2}e^{if_{4jy}y_j}e^{if_{4z}z_j}\left(2\pi d_j^2\right)^{3/2}\sum_{n,n',n_\delta,n'_\delta} e^{ig_m}J_m$$
$$\times\Bigg[Fe^{-q_m^2d_j^2/2}e^{iq_mx_j} + \frac{1}{2}\{e^{i(q_m+k_x)x_j}e^{-\frac{1}{2}(q_m+k_x)^2d_j^2}e^{-i\omega t_0}(f_2+f_{2\delta}e^{-i\delta}) + e^{i(q_m-k_x)x_j}e^{-\frac{1}{2}(q_m-k_x)^2d_j^2}e^{i\omega t_0}(f_2+f_{2\delta}e^{i\delta})\}$$
$$+\frac{1}{4}\{e^{i(q_m+2k_x)x_j}e^{-\frac{1}{2}(q_m+2k_x)^2d_j^2}e^{-i2\omega t_0}F_3^- + e^{i(q_m-2k_x)x_j}e^{-\frac{1}{2}(q_m-2k_x)^2d_j^2}e^{i2\omega t_0}F_3^+\}\Bigg] \tag{31}$$

where

$$q_m = f_{4jx}^{\mp} - Mk_x, \tag{32}$$

$$M = n + 2n' + n_\delta + 2n'_\delta, \tag{33}$$

$$g_m = M\omega t_0 + (n_\delta + 2n'_\delta)\delta, \tag{34}$$

$$J_m = J_n(f_5)J_N(f_6)J_N(f_{5\delta})J_N(f_{6\delta}), \tag{35}$$

$$F = f_1 + \tfrac{1}{2}f_3 + \tfrac{1}{2}f_{3\delta} + \tfrac{1}{2}f_{23}\cos\delta, \tag{36}$$

$$F_3^{\pm} = f_3 + f_{3\delta}e^{\pm i2\delta} + f_{23}e^{\pm i\delta}. \tag{37}$$

Note that although Eq. (31) is a nice analytical expression it has fourfold summations involving the Bessel functions and this is a major factor which makes the computational process much slower compared to direct numerical integration of the integral using Eq. (29). The step for x in the integral of Eq. (29) has to be several times smaller than $\pi/\max|f_{4x}|$ to obtain correct results. It is more efficient to evaluate the coefficient $c^s(\mathbf{p})$ numerically than to do it analytically because analytical expression involves a fourfold infinite series that would be too computationally expensive. The coefficients f_1, f_{2d}, f_{3d}, and f_{23} in Eq. (29) are most efficiently found numerically by multiplying the two vectors, e.g., Eqs. (27) and (28).

IV. MOMENTUM SQUEEZING ANALYSIS

Using the dipole approximation by setting $x = x_j$ in Eqs. (3) and (6) and keeping only the linear terms $x - x_j$ in the Taylor expansion of the $S^{\pm}$ functions will allow us to evaluate the integration over x from the previous section. Thus we will obtain simple expressions which will help us to interpret squeezing in the momentum spectra obtained in the previous section via numerical integration.

Let us separate out the x-dependent term $\Xi(x)$ in the phase factor

$$-S^{\pm}(\mathbf{p};\varphi_0) + S^{+}(\mathbf{p}_j,\varphi_0) = \frac{(\pm E - E_j)t_0}{\hbar} - \frac{(\pm p_y - p_{jy})y}{\hbar} - \frac{(\pm p_z - p_{jz})z}{\hbar} + \Xi(x) \tag{38}$$

and define it as

$$\Xi(x) = -\frac{(\pm p_x - p_{jx})x}{\hbar} + \frac{1}{\hbar}\int_{-\infty}^{k\cdot x_0} e\mathbf{Q}\cdot\mathbf{A}(\varphi')d\varphi'$$
$$-\frac{1}{\hbar}\int_{-\infty}^{k\cdot x_0} W_{j\mp}\frac{1}{2}e^2|\mathbf{A}(\varphi')|^2 d\varphi'$$
$$= -\frac{(\pm p_x - p_{jx})(x'+x_j)}{\hbar} + \frac{1}{\hbar}\int_{-\infty}^{\omega t_0 - k_x(x'+x_j)}\Big[e\mathbf{Q}\cdot\mathbf{A}(\varphi') - W_{j\mp}\frac{1}{2}e^2|\mathbf{A}(\varphi')|^2\Big]d\varphi' \tag{39}$$

where $\mathbf{Q} = \frac{\mathbf{p}_j}{k\cdot p_j} - \frac{\mathbf{p}}{k\cdot p} = (-\Delta_{jy}, -\Delta_{jz}) = \frac{\mathbf{p}_j - \mathbf{p}}{k\cdot p_j} + \frac{\mathbf{p}}{k\cdot p_j} - \frac{\mathbf{p}}{k\cdot p} = \mathbf{p}W_{j-} - \frac{\mathbf{p}-\mathbf{p}_j}{k\cdot p_j}$ and the relative coordinate $x' = (x - x_j)$. We set $\phi = 0$, so $A\cdot p = -\mathbf{A}\cdot\mathbf{p}$ and $A^2 = -|\mathbf{A}|^2$. Alternatively, the x-dependent phase factor $e^{if_{4jx}^{\mp}x + i\sum_{d=0,\delta}\{f_{5jd}\sin(\varphi_0+d) + f_{6jd}^{\mp}\sin 2(\varphi_0+d)\}}$ in the integral of Eq. (29) is defined as

$$\Xi(x) = f_{4jx}^{\mp}x + \sum_{d=0,\delta}\{f_{5jd}\sin(\varphi_0+d) + f_{6jd}^{\mp}\sin 2(\varphi_0+d)\}. \tag{40}$$

The integral over x (for the positive-energy case) can be evaluated and the squeezing effect can be understood by obtaining an approximate analytical expression through Taylor expansion around x_j for $\sin(\omega t_0 - k_x x) = \sin(\omega t_0 - k_x x_j) - k_x(x - x_j)\cos(\omega t_0 - k_x x_j)$ in the phase of Eq. (29), which becomes

$$\int_{-\infty}^{\infty} e^{-(x-x_j)^2/2d_j^2}e^{i\Xi(x)}dx = e^{i\Xi(x_j)}\int_{-\infty}^{\infty} e^{-x'^2/2d_j^2}e^{iG_jx'}dx'$$
$$= \frac{e^{i\Xi(x_j)}}{a\sqrt{2}}e^{-G_j^2/4a^2}$$
$$= e^{i\Xi(x_j)}d_je^{-G_j^2d_j^2/2} \tag{41}$$

where

$$\Xi(x) \approx \Xi(x_j) + G_jx', \tag{42}$$

$$\Xi(x_j) = f_{4jx}^{\mp}x_j + \sum_{d=0,\delta}\{f_{5jd}\sin(\theta_j+d) + f_{6jd}^{\mp}\sin 2(\theta_j+d)\}, \tag{43}$$

$$G_j = f_{4jx}^{-} - k_x\sum_{d=0,\delta}\{f_{5jd}\cos(\theta_j+d) + f_{6jd}^{\mp}2\cos 2(\theta_j+d)\} \tag{44}$$

with $\theta_j = \omega t_0 - k_x x_j$.

An alternative expression suited for further analysis is

$$\Xi(x_j) = -\frac{(\pm p_x - p_{jx})x_j}{\hbar} + \frac{1}{\hbar}\int_{-\infty}^{\theta_j=\omega t_0 - k_x x_j} \times \left[e\mathbf{Q}\cdot\mathbf{A}(\varphi') - W_{j\mp}\frac{1}{2}e^2|\mathbf{A}(\varphi')|^2\right]d\varphi'. \quad (45)$$

Using Leibniz's rule and considering the positive-energy case,

$$G_j = \frac{d\,\Xi(x')}{dx'} = \frac{d\,\Xi(x')}{d\varphi_0}\frac{d\varphi_0}{dx'} = -\frac{(p_x - p_{jx})}{\hbar} - \frac{1}{\hbar}k_x\left[e\mathbf{Q}\cdot\mathbf{A}(\theta_j) - W_{j-}\frac{1}{2}e^2|\mathbf{A}(\theta_j)|^2\right] \quad (46)$$

$$= -\frac{(p_x - p_{jx})}{\hbar} + \frac{1}{\hbar}k_x\frac{(\mathbf{p}-\mathbf{p}_j)\cdot e\mathbf{A}(\theta_j)}{(k\cdot p_j)} - \frac{1}{\hbar}k_x W_{j-}\chi \quad (47)$$

and the nonlinearity in the squeezing is governed by

$$\chi = e\mathbf{p}\cdot\mathbf{A}(\theta_j) - \frac{e^2|\mathbf{A}(\theta_j)|^2}{2}. \quad (48)$$

An alternative expression is

$$\hbar G_j = -(p_x - p_{jx}) + k_x\left[\frac{\mathbf{p}}{k\cdot p} - \frac{\mathbf{p}_j}{k\cdot p_j}\right]\cdot e\mathbf{A} + k_x\left(\frac{1}{k\cdot p_j} - \frac{1}{k\cdot p}\right)\frac{e^2|\mathbf{A}(\theta_j)|^2}{2}. \quad (49)$$

Using $k\cdot p = \frac{\omega}{c}\frac{E}{c} - k_x p_x$ and the Taylor expansions around $p_{jq}(q = x, y, z)$ we have

$$E - E_j \simeq \frac{(\mathbf{p}-\mathbf{p}_j)\cdot(2\mathbf{p}_j + p - p_j)}{2m} \simeq \frac{1}{m}(\mathbf{p}-\mathbf{p}_j)\cdot\mathbf{p}_j + \frac{|\mathbf{p}-\mathbf{p}_j|^2}{2m}, \quad (50)$$

$$W_{j-}(\mathbf{p},\mathbf{p}_j) = \frac{\omega(E-E_j)/c^2 - k_x(p_x - p_{jx})}{(k\cdot p_j)(k\cdot p)} \simeq \frac{\frac{\omega}{c}\frac{1}{mc}(\mathbf{p}-\mathbf{p}_j)\cdot\mathbf{p}_j + \frac{\omega}{c}\frac{|\mathbf{p}-\mathbf{p}_j|^2}{2mc} - k_x(p_x - p_{jx})}{(k\cdot p_j)^2}. \quad (51)$$

After rearranging the terms, Eq. (44) or Eq. (46) can be rewritten as

$$\hbar G_j = -(p_x - p_{jx})\left[1 - \frac{k_x\xi}{k\cdot p_j}\left(1 - \frac{p_{jx}}{\epsilon mc}\right)\right] + \frac{k_x(\mathbf{p}-\mathbf{p}_j)}{k\cdot p_j}\cdot\left[e\mathbf{A}(\theta_j) - \frac{\mathbf{p}_{j\perp}}{\epsilon mc}\xi\right] - H \quad (52)$$

where $\mathbf{p}_{j\perp} = [0, p_{jy}, p_{jz}]$ and

$$\xi = \frac{k_x}{(k\cdot p_j)}\chi(\mathbf{p}_j) \simeq \epsilon\left(1 + \frac{cp_{jx}}{E_j}\right)\frac{c}{E_j} \times \left[e\mathbf{p}_j\cdot\mathbf{A}(\theta_j) - \frac{e^2|\mathbf{A}(\theta_j)|^2}{2}\right], \quad (53)$$

$$H = \frac{\frac{\omega}{c}}{k\cdot p_j}\frac{|\mathbf{p}-\mathbf{p}_j|^2}{2mc}\xi + \left(\frac{\frac{\omega}{c}(\mathbf{p}-\mathbf{p}_j)\cdot\frac{\mathbf{p}_j}{mc}}{k\cdot p_j} - \frac{k_x(p_x - p_{jx})}{k\cdot p_j}\right) \times \left(\frac{k_x(\mathbf{p}-\mathbf{p}_j)}{k\cdot p_j}\cdot e\mathbf{A}(\theta_j)\right). \quad (54)$$

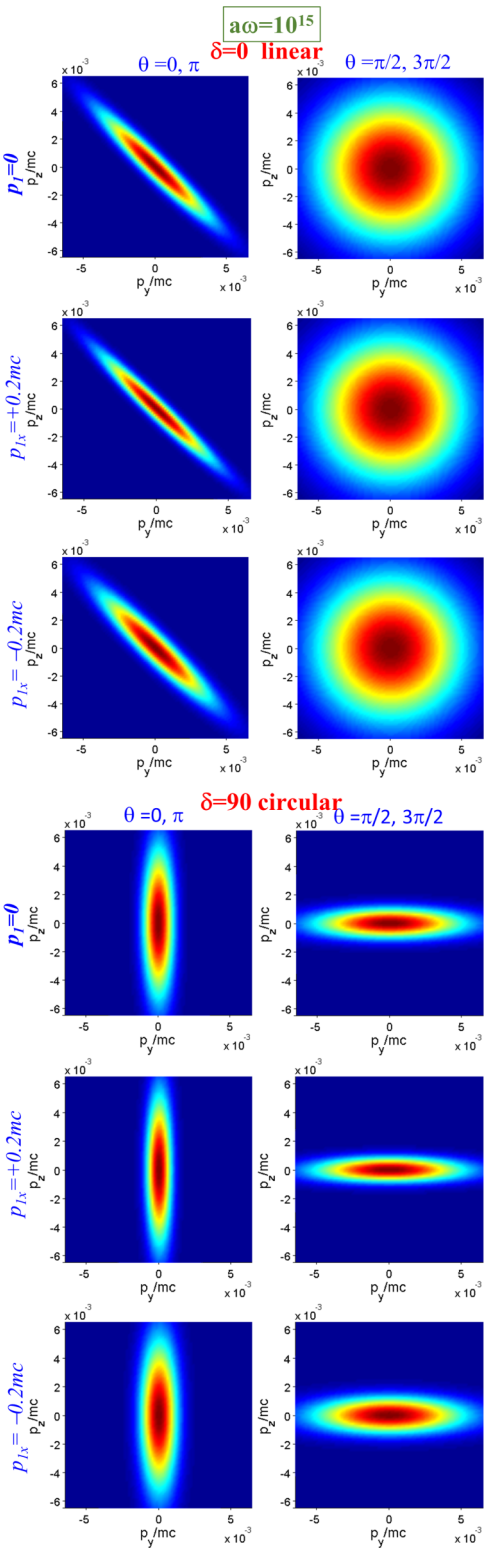

FIG. 2. Distributions of the $\Sigma_{s=1:4}|c^s(\mathbf{p})|^2$ on the y-z momentum plane for electron initial momenta $\mathbf{p}_1 = 0$ and at $p_{1x} = \pm 0.2mc$ for linear ($\delta = 0^\circ$) and circular ($\delta = 90^\circ$) polarization lasers.

Equation (52) is the main analytical expression for further analysis, containing the linear terms in $p_q - p_{jq}$, and the quadratic terms in $p_q - p_{jq}$ are contained in H. The important scalar product $(\mathbf{p}-\mathbf{p}_j)\cdot\mathbf{V}$ in the second term of Eq. (52),

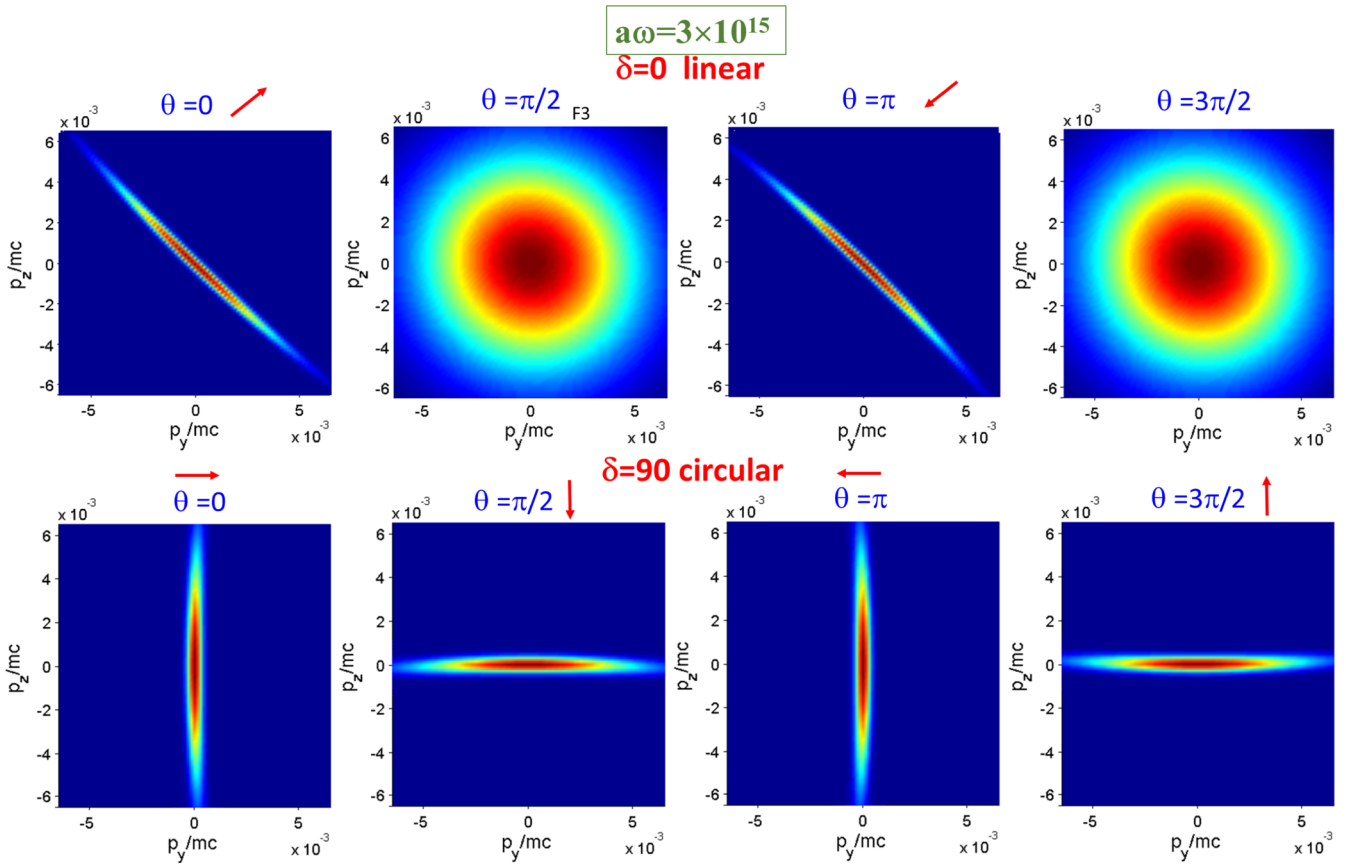

FIG. 3. Distributions of the $\Sigma_{s=1:4}|c^s(\mathbf{p})|^2$ on the y-z momentum plane for electron initial momenta $\mathbf{p}_1 = \mathbf{0}$ for stronger laser fields. The arrows on top show the direction of the vector potential for the respective θ.

with the vector (illustrated in Fig. 1)

$$\mathbf{V} = e\mathbf{A}(\theta_j) - \frac{\mathbf{p}_{j\perp}}{\epsilon mc}\xi = (0, V_y, V_z), \tag{55}$$

clearly explains the features such as rotation and squeezing seen in all the plots presented in the next subsections that are obtained from the exact equations above. Note that rotation and squeezing are controlled by $\mathbf{V}$, particularly ξ and the relative direction of both vectors $\mathbf{p}_{j\perp}$ and $\mathbf{A}(\theta_j)$, which are on the y-z plane or polarization plane.

A. Squeezing

If $\mathbf{p}_{j\perp} = 0$ is finite but *parallel* to $\mathbf{A}$, the squeezed momentum distribution is orthogonal to $\mathbf{A}(\theta_j)$. Squeezing occurs along $\mathbf{A}(\theta_j)$ but there is no squeezing in the direction perpendicular to $\mathbf{A}(\theta_j)$. There are two interesting cases when squeezing in a certain direction does not occur for specific field values. First, when the two vectors $\mathbf{A}$ and $\mathbf{p}_{j\perp}$ are *antiparallel*, at a specific value of the laser field they may cancel and $\mathbf{V}$ is zero. In this case, V_y and V_z are zero or $eA_u \simeq \beta_{ju}\xi$, so no (transverse) squeezing occurs along $\mathbf{p}_{j\perp}$ or in the polarization plane but may occur in the p_x direction. In the second case, at a specific field intensity such that ξ is zero no squeezing will occur in the p_x direction but may occur in the direction of $\mathbf{p}_{j\perp}$ only.

B. Rotation

When the initial momentum vector $\mathbf{p}_{j\perp}$ is finite and parallel to the vector $\mathbf{A}(\theta_j)$, the squeezed momentum distribution is orthogonal to $\mathbf{A}(\theta_j)$, i.e., the distribution is not rotated. The strength of rotation strongly depends on the magnitude of the ξ parameter and the relative direction of both vectors $\mathbf{p}_{j\perp}$ and $\mathbf{A}$. The strongest rotation occurs when $\mathbf{p}_{j\perp}$ is perpendicular to $\mathbf{A}(\theta_j)$. Strong rotations will occur when the direction of $\mathbf{V}$ in Eq. (52) differs significantly from the direction of $\mathbf{A}$.

A specific situation in which the squeezing and rotation can be easily understood is when the initial momentum $\mathbf{p}_j = 0$ (in Figs. 2 and 3). Here, ξ simplifies to

$$\xi = -\frac{|e\mathbf{A}(\theta_j)|^2}{2mc} \tag{56}$$

and the lowest-order approximation predicts that

$$\hbar G_j = -p_x\left(1 + \frac{|e\mathbf{A}(\theta_j)|^2}{2m^2c^2}\right) + \frac{\mathbf{p}\cdot\mathbf{A}(\theta_j)}{mc} \tag{57}$$

where G_j^2 is proportional to $(\mathbf{p}\cdot\mathbf{A})^2$, which is symmetric with respect to the direction of the $\mathbf{A}$ vector. We assume $\epsilon = \frac{ck_x}{\omega} \simeq 1$ and $E_j \simeq mc^2$ in Eqs. (52) and (53). By keeping higher-order momentum terms in Eq. (52) we obtain $G_j^2 \sim [\frac{\mathbf{p}}{mc}\cdot e\mathbf{A}(1+\frac{p_x}{mc}) + (\frac{|\mathbf{p}||\mathbf{A}|}{2mc})^2]^2$ leading to bending observed at high laser intensities in the next section.

As we will show in Fig. 3 the plot for a certain value $\theta(= 0, \pi/2)$ is slightly different from $\theta + \pi(= \pi, 3\pi/2)$. This

asymmetry arises from $\frac{\mathbf{p}}{mc}\cdot e\mathbf{A}+(\frac{|\mathbf{p}||\mathbf{A}|}{2mc})^2$ as a whole and cannot be due to the quadratic field term alone, which is symmetric since

$$\frac{e^2|\mathbf{A}(\theta_j)|^2}{2}=\left(\frac{ea_y}{2}\right)^2(1+\cos 2\theta_j)+\left(\frac{ea_z}{2}\right)^2[1+\cos 2(\theta_j+\delta)]. \quad (58)$$

Analytical expressions of G_j for analysis of momentum distribution for cases of finite p_{jq} in the figures are given in Appendix C.

C. Angle of rotational α

The momentum distribution on the y-z plane is governed by $(\mathbf{p}_\perp-\mathbf{p}_{j_\perp})\cdot\mathbf{V}$, the second term of Eq. (52), which can be viewed as rotated momentum expressed by

$$(p_y-p_{jy})V\cos\tilde{\alpha}+(p_z-p_{jz})V\sin\tilde{\alpha}=|\mathbf{p}_\perp-\mathbf{p}_{j_\perp}|V\cos\mathcal{A}. \quad (59)$$

Here, $V=\sqrt{V_z^2+V_y^2}$, $\mathcal{A}$ is the angle for the dot product, and $\alpha=\tilde{\alpha}+90^\circ$ is the rotational angle of the squeezed momentum distribution relative to the (horizontal) y axis, as illustrated in Fig. 1 and defined through

$$\tan(\alpha-90^\circ)=\tan\tilde{\alpha}=\frac{V_z}{V_y}=\frac{ea_z\cos(\theta_j+\delta)-\beta_{jz}\xi}{ea_y\cos\theta_j-\beta_{jy}\xi}, \quad (60)$$

$$\xi\simeq(1+\beta_{jx})\left(\boldsymbol{\beta}_{j\perp}\cdot e\mathbf{A}(\theta_j)-\frac{e^2|\mathbf{A}(\theta_j)|^2}{2mc}\right) \quad (61)$$

where $\boldsymbol{\beta}_{j\perp}=(0,\frac{p_{jy}}{mc},\frac{p_{jz}}{mc})$. So, squeezing is largest in the direction of the vector $\mathbf{V}$.

Writing out all the momentum components linear in $(\mathbf{p}-\mathbf{p}_j)$ in Eq. (52), we see the contribution of a fraction $\frac{p_{ju}}{mc}$ of the momentum ξ through

$$\hbar G_j=(p_x-p_{jx})\left[\frac{k_x\xi}{k\cdot p_j}\left(1-\frac{\beta_{jx}}{\epsilon}\right)-1\right]+\frac{k_xV}{k\cdot p_j}(p_\perp-p_{j_\perp}). \quad (62)$$

For weak field $|e\mathbf{A}(\theta_j)|<<|\mathbf{p}_j|$ (constrained by $|p_j|<mc$) the first term of ξ [Eq. (61)] which dominates is in the order of $\beta_{ju}eA_u$, $u=y,z$, so the momentum width of the x component is essentially affected by the laser fields only if p_{jy} or p_{jz} is relativistic. For sufficiently high laser intensities such that $|e\mathbf{A}(\theta_j)|\gg|\mathbf{p}_j|$, the value of p_{jy} or p_{jz} has little effect on the momentum width of the x component since the second term of ξ dominates, and $\xi\simeq-(1+\beta_{jx})\frac{|e\mathbf{A}(\theta_j)|^2}{2mc}$ is negative and $\mathbf{V}\simeq e\mathbf{A}(\theta_j)+\boldsymbol{\beta}_{j\perp}\frac{|e\mathbf{A}(\theta_j)|^2}{2mc}$.

D. Momentum width

The arguments in $e^{-G_j^2d_j^2/2}e^{-f_{4jy}^{\mp}{}^2d_j^2/2}e^{-f_{4jz}^{\mp}{}^2d_j^2/2}$ can be combined to form the 3D Gaussian $\exp[-(p_x-p_{jx})^2/\sigma_{jx}^2-(p_\perp-p_{j_\perp})^2/\sigma_{j\perp}^2]$ with the variances

$$\sigma_{jx}^2=\frac{2\hbar^2}{d_j^2\left[1-\frac{k_x}{(k\cdot p_j)}\xi\right]^2}, \quad (63)$$

$$\sigma_{j\perp}^2=\frac{2\hbar^2}{d_j^2\left[1+\frac{k_x}{k\cdot p_j}\sqrt{\{ea_y\cos\theta_j-\beta_{jy}\xi\}^2+\{ea_z\cos(\theta_j+\delta)-\beta_{jz}\xi\}^2}\right]}, \quad (64)$$

which shows the momentum widths reduce with increase of a_y,a_z and oscillate with $\theta_j=\omega t_0-k_xx_j$ and not just ωt_0. The "transverse" squeezing in the y-z plane can be clearly seen from the figures with momentum widths given by the approximate analytical expression Eq. (64). If $\delta=0$ and $a_y=a_z$ we have $\sigma_{jy}=\sigma_{jz}$ and Eq. (64) simplifies. We also have "longitudinal" squeezing along the x direction according to Eq. (63). However, the squeezing effect is different where the variance has quartic dependence on the field components, a_y and a_z, while the variance of the transverse (y and z) components has quadratic dependence on the field components (due to the square root).

The longitudinal momentum squeezing is related to the kinetic effect of the Lorentz force that is unfavorable for recollision in the high-order harmonic generation (HHG) process and can be overcome by using counterpropagating equal-handed circularly polarized laser pulses [23]. Such laser configuration is shown to produce very high spatial squeezing and electron current when the time for a round trip in the transverse y-z plane is equal to the electron excursion time along the x axis which would enhance the intensity of high-harmonic generation. The influence of the magnetic field is equally as important as the electric field on the electron kinetics in the HHG process and can be controlled in different ways, by harmonic fields [24] or static magnetic fields, to counteract the relativistic kinetic effect of the magnetic part of the laser field to achieve higher intensity [25] and a broader HHG plateau [26].

V. RESULTS AND DISCUSSIONS

Using Eqs. (16)–(29) we have plotted the space- and time-independent momentum distribution $\sum_{s=1}^4|c^s(\mathbf{p})|^2$ for linearly and circularly polarized laser fields. We use the following default parameters unless stated otherwise: $a\omega=10^{15}\,\mathrm{V\,m^{-1}}$, $a_y=a_z=\sqrt{0.5}a$, $\delta=90$, and the initial momenta have magnitude $|p_{jq}|=0.2mc$ where $q=x,y,z$, with two possible signs for the momentum, giving four possibilities for each q. The corresponding $\frac{ea_y}{mc}$ is -5 (negative due to electron charge), which is much greater than $\frac{|p_{jq}|}{mc}=0.2$, hence ξ is negative.

Here, $\omega=2c/(137a_B)$ where $a_B=0.5292\times10^{-10}$ m is the Bohr radius. Hence, the intensity is $((c\varepsilon_o)/2)(a\omega)^2=1.327\times10^{27}\ \mathrm{Wm^{-2}}$. The central position of the single-electron case is $x_1=0$ while superposed electron states are fixed at $x_1=-30d$ and $x_2=+30d$, with $d=\sqrt{2}a_B$. For

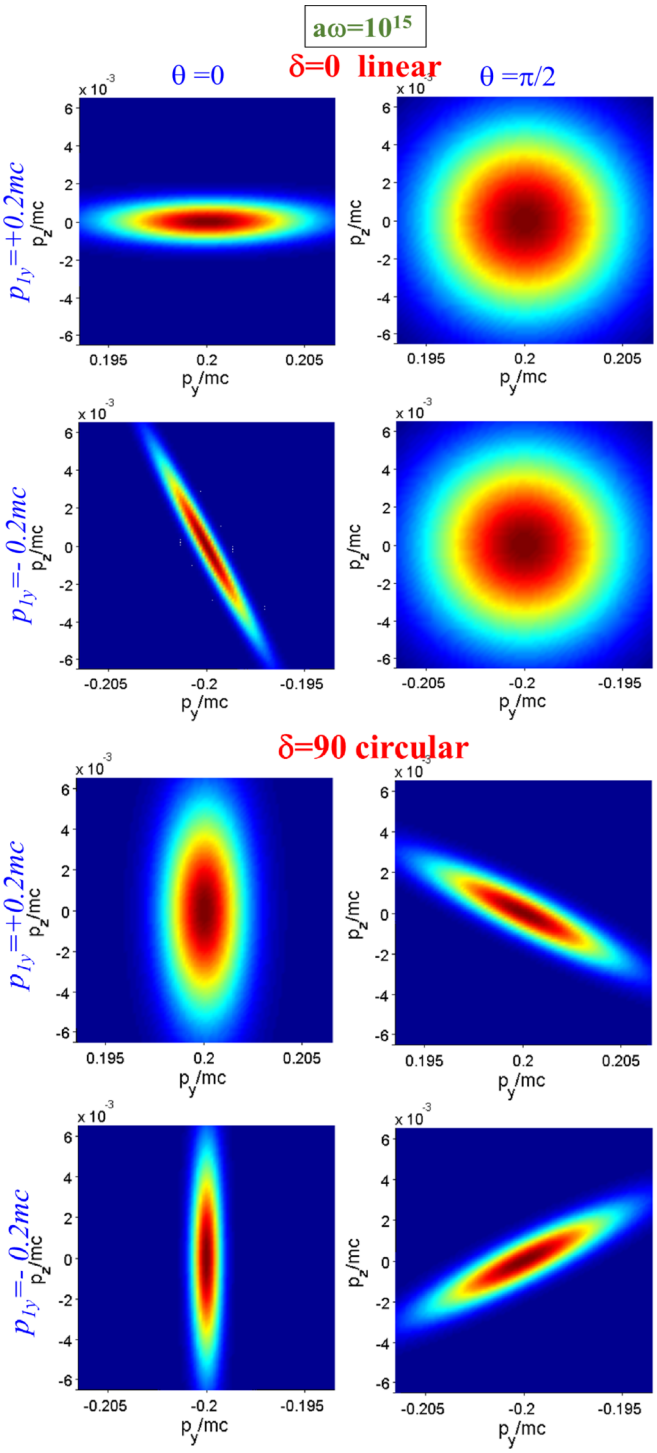

FIG. 4. Distributions of the $\Sigma_{s=1:4}|c^s(\mathbf{p})|^2$ on the y-z momentum plane at $p_x = p_{1x}$ for linearly ($\delta = 0^\circ$) and circularly ($\delta = 90^\circ$) polarized lasers for the electron initial momenta along the y direction.

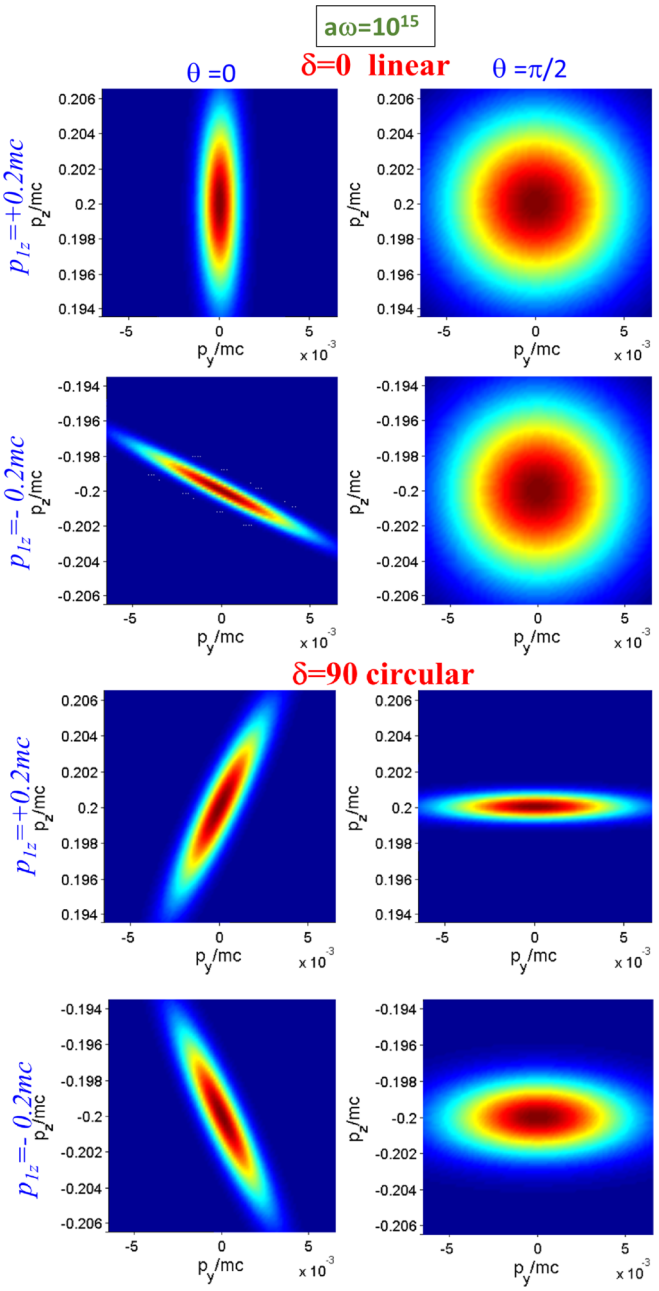

FIG. 5. Distributions of the $\Sigma_{s=1:4}|c^s(\mathbf{p})|^2$ on the y-z momentum plane at $p_x = p_{1x}$ for linearly ($\delta = 0^\circ$) and circularly ($\delta = 90^\circ$) polarized lasers for the electron initial momenta along the z direction.

initial superposed states plotted in Figs. 7–9, we set initial time $t_0 = T/4$, $T = 2\pi/\omega$, and relative phase $\Phi = 0$.

For the plots in the y-z momentum plane, we fix $p_x = p_{1x}$ while for the x-y momentum plane we fix $p_z = p_{1z}$. By default, $p_{1x} = p_{1y} = p_{1z} = 0$, unless stated otherwise. Note that all the plots of momentum distributions are for the spin-up electron only. The possible physical variables that can be controlled in computations are (a) laser parameters ω, a, a_y/a_z, δ; (b) electron wave-packet initial mean position $\mathbf{r}_j$, mean momentum $\mathbf{p}_j$, and width d_j; (c) momentum plane $p_y - p_z$, $p_z - p_x$, or $p_x - p_y$; and (d) current time t and initial time t_0. However, x_j and t_0 are connected by the variable $\theta_j = \omega t_0 - k_x x_j$. Thus we have chosen to plot the distributions versus different values of θ_j, electron mean momenta p_{1x}, p_{1y}, and p_{1z} and laser field polarizations. We define the laser field vector potentials; $\mathbf{A} = \frac{a}{\sqrt{2}}(\hat{y} + \hat{z})\cos\theta_j$ for linear polarization and $\mathbf{A} = \frac{a}{\sqrt{2}}(\hat{y}\cos\theta_j - \hat{z}\sin\theta_j)$ for circular polarization. In other words, the momentum distribution depends on the (initial) local field experienced by the electron at position x_j

at instant t_0 with the momentum $\mathbf{p}_j$. This explains why the momentum distribution depends strongly on θ_j, as shown in Fig. 2 for a single state (no superposition) with initial momentum $\mathbf{p}_1 = 0$, a situation which allows simple physical explanation. The dependency of the orientation or rotational angle of the momentum distributions on θ_j in the figures agrees with the analytical prediction of Eq. (60).

Figure 2 shows that linear polarization makes the momentum squeezing orientation in the z-y plane that depends on θ_j. Here, the rotational angle α_x satisfies

$$\tan(\alpha_x - \pi/2) = \frac{\cos(\theta_j + \delta)}{\cos\theta_j}. \tag{65}$$

Circular polarization makes the squeezing orientation along the z direction for $\theta_j = 0$ and rotates 90° to squeezing orientation along the y direction for $\theta_j = \pi/2$. Finite momentum along x has no effect on the orientation of squeezing but for positive momentum it is slightly narrower and for negative momentum it is slightly broader, due to terms nonlinear in $(p_x - p_{jx})$. The stronger field strength of $a\omega = 3 \times 10^{15}\,\mathrm{V\,m^{-1}}$ gives narrower squeezing but the orientation is not changed, as shown in Fig. 3 for zero mean momentum. However, we notice remarkable features; there is a difference between the squeezed distributions for $\theta_j = 0$ and π (for both polarizations) as well as between $\theta_j = \pi/2$ and $3\pi/2$ (for circular polarization) in terms of the slight bending of distributions. A closer observation reveals that, for circular polarization, the distribution for $\theta_j = 0$ is a reflection of the case $\theta_j = \pi$ at $y = 0$ while the distribution for $\theta_j = \pi/2$ is a reflection of the case $\theta_j = 3\pi/2$ at $z = 0$. The results are qualitatively the same for finite mean momentum. The analytical expression we derived suggests that nonlinearity in the momentum due to relativistic effect is responsible for the bending of the distributions.

In Fig. 4, the distribution for θ_j with a particular value p_{1y} is the same as the distribution for $\theta_j + \pi$ with value $-|p_{1y}|$, and this is true for any polarization. Therefore the plots for $\theta_j = \pi$ and $3\pi/2$ are not shown. The rotational angle α_y satisfies

$$\tan(\alpha_y - \pi/2) = \frac{\cos(\theta_j + \delta)}{\cos\theta_j - 0.2\left\{0.2\cos\theta_j + \left(\frac{5}{4}\right)[2 + \cos 2\theta_j + \cos 2(\theta_j + \delta)]\right\}}. \tag{66}$$

Similarly, Fig. 5 shows the distribution for θ_j with values of p_{1z} is the same as the distribution for $\theta_j + \pi$ with values $-|p_{1z}|$ for any polarization, with the rotational angle α_z given by

$$\tan(\alpha_z - \pi/2) = \frac{\cos(\theta_j + \delta) - 0.2\left\{0.2\cos(\theta_j + \delta) + \left(\frac{5}{4}\right)[2 + \cos 2\theta_j + \cos 2(\theta_j + \delta)]\right\}}{\cos\theta_j}. \tag{67}$$

For stronger field, the squeezing orientation changes significantly. For linear polarization with $\theta_j = 0$ and $p_{1z} = +0.2mc$ instead of vertical, the distribution becomes slanted to 45° when the laser field increases.

For linear polarization, the momentum distributions in the y-z plane show no squeezing at $\theta_j = \pi/2$ and $3\pi/2$ regardless of initial momentum since it corresponds to zero field $\mathbf{A} = \frac{a}{\sqrt{2}}(\hat{y} + \hat{z})\cos\ \theta_j$. This shows that the vector potential, or the electric field, is behind the momentum squeezing. For circular polarization, the squeezing along the y axis only when $\theta_j = 0, \pi$ is due to the term $\frac{k_x}{(k\cdot p_j)} a_y \cos\ \theta_j$ in Eq. (52) while the squeezing along the z axis only when $\theta_j = \pi/2, 3\pi/2$ is due to the term $\frac{k_x}{(k\cdot p_j)} a_z \sin\ \theta_j$. A similar explanation applies to momentum distributions in the x-y plane in Fig. 6.

The squeezed distribution in Fig. 2 is tilted along 135° relative to the p_y axis for $p_{1x} = \pm 0.2mc$ where the electron moves normal to the y-z momentum plane with a linear polarized laser ($\delta = 0$) corresponding to the electric field at 45° to the p_y axis. This shows that the electric field squeezes the electron distribution along this direction. However, the squeezed distribution for circular polarizations is aligned to a fixed angle since the y and z components no longer exert the same effect but depend on θ_j through $\mathbf{A} = \frac{a}{\sqrt{2}}(\hat{y}\cos\theta_j - \hat{z}\sin\theta_j)$. For an electron moving along $+y$ $(-y)$, the momentum width in the y direction is increased (reduced). This asymmetry indicates the importance of the electric-field direction relative to the direction of a moving electron. The case is similar for an electron moving along $+z$ $(-z)$ due to symmetry. For the x-y momentum plane, the features in the distributions in Fig. 6 can be explained in the same manner but the rotational angle has to be determined by the ratio $\frac{\xi\{1-\beta_{jx}/\epsilon\}}{V}$.

A. Superposed spins in the y-z momentum plane

By comparing the results in subsequent figures with a single state we can identify the features due to superposition of two initial electron states. For $t_0 = T/4$ the factor in the laser field has two values corresponding to the state at x_1 (upper sign) and the state at x_2 (lower sign): $\cos\theta_j = \cos(\pi/2 \pm 30k_x d) = \mp\sin 30k_x d$ (for linear), that gives discernible rotations in the momentum distributions on the y-z momentum plane (normal to the laser propagation direction) in Fig. 7 . But only one value $\cos(\theta_j + \pi/2) = -\cos(30k_x d)$ for circular polarization.

This explains why we find the "X" (crossed) distributions only when the two initial momenta are in the same direction, which is essentially the crossings of two squeezed and rotated wave packets. When both states of the electron initially move in opposite directions $p_{1q} = -p_{2q}$ there is only one squeezed distribution (not shown). This happens for initial momenta in x, y, and z directions.

When the superposed electron states initially move opposite to the laser direction, $p_{1x} = p_{2x} = -0.2mc$, the squeezing of the X distribution is reduced due to the relative direction of the wave vector and the electron, a rather counterintuitive effect. The strong squeezing in the distributions is due to relativistic effect of the field on the electron.

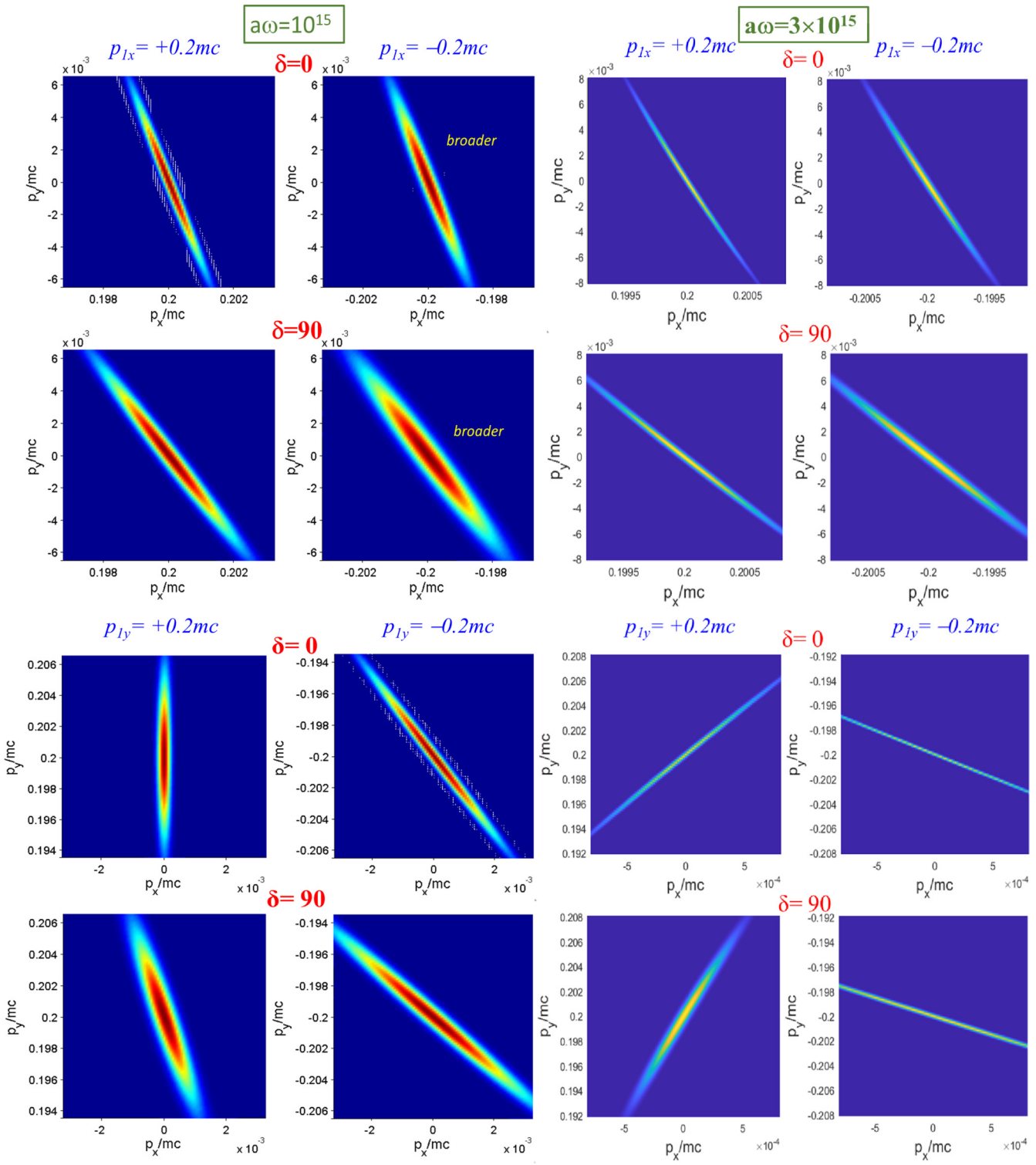

FIG. 6. Distributions of the $\Sigma_{s=1:4}|c^s(\mathbf{p})|^2$ on the x-y momentum plane at $p_x = p_{1x}$ for linearly ($\delta = 0^\circ$) and circularly ($\delta = 90^\circ$) polarized lasers for the electron initial momenta along x, y, and z directions. Here, $\theta = 0$.

For initial momenta along the x direction (finite p_{jx}) with linear polarized laser fields ($\delta = 0$) there is no X distribution for all the four cases' initial momenta since $\frac{V_z}{V_y} = \frac{\cos(\theta_j+\delta)}{\cos\theta_j} \to 1$. The X distribution is present for circular polarization because $\frac{V_z}{V_y} = \frac{-\sin\theta_j}{\cos\theta_j}$ would depend on different electron initial position x_j. More importantly, the dependence on the directionality of the initial momentum is connected to the effect of the spin direction relative to the photon polarization.

When the initial momentum is along the y direction with strong field, there is also crossing of two squeezed wave packets, but for both polarizations. For linear polarization (Fig. 7), the resulting X distributions appear rotated, cross each other at a small angle, are nonsymmetric with respect

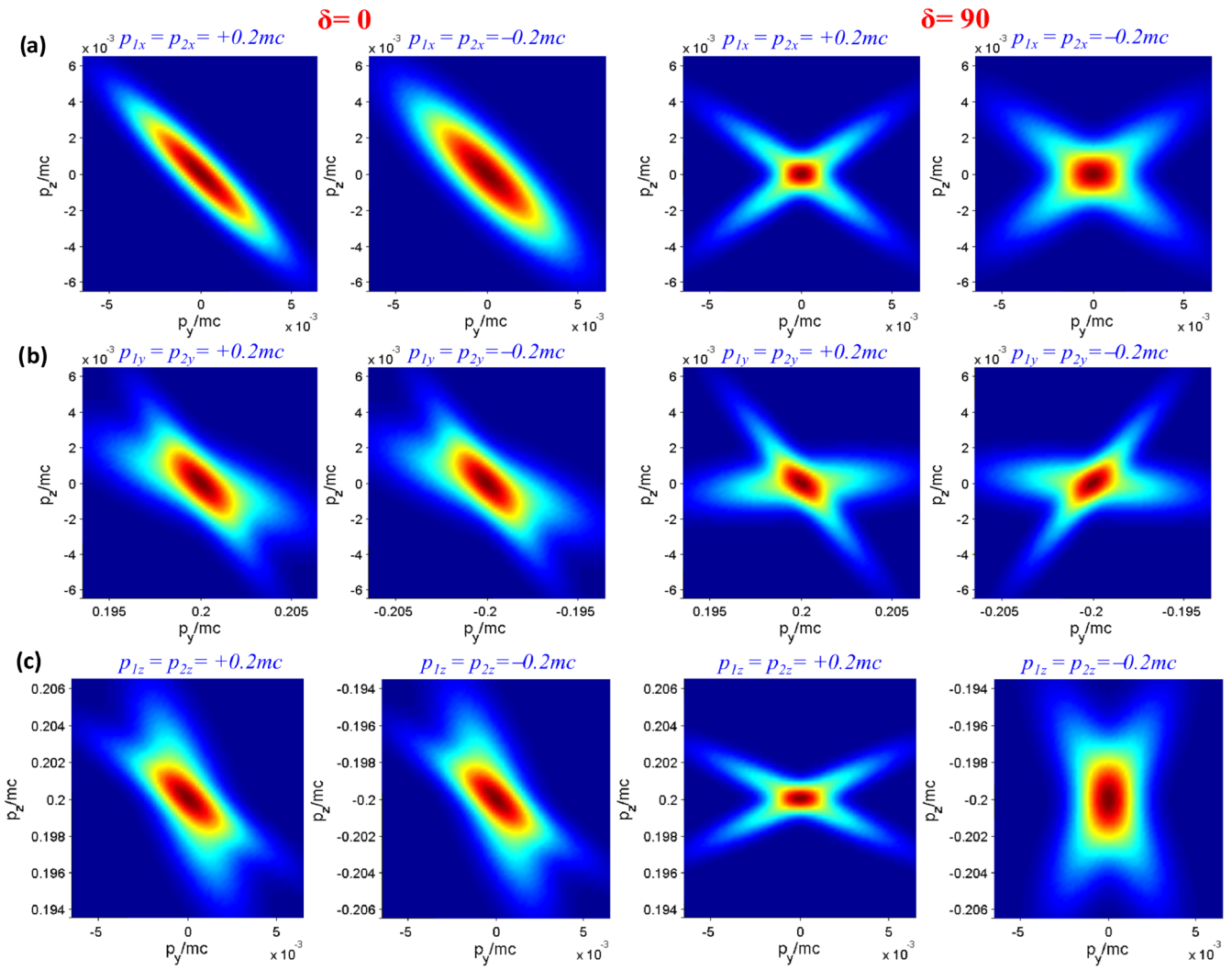

FIG. 7. Distributions $\Sigma_{s=1:4}|c^s(\mathbf{p})|^2$ on the y-z momentum plane at $p_z = p_{1x}$ for an electron in the superposed state driven by linearly polarized ($\delta = 0^\circ$) and circularly polarized ($\delta = 90^\circ$) lasers. Everything else is the same as in Eq. (8).

to the axes, and are also not symmetric upon reflection at point $p_{y,z} = 0$. The distributions are identical for positive and negative values of $p_{1y} = p_{2y}$, unaffected by the momentum direction relative to the laser wave vector. The results are qualitatively similar for the case $p_{1z} = p_{2z}$. However, for right-circular polarization ($\delta = +90$), the distributions are the image reflections at $p_y = 0$ (and not $p_z = 0$) of the left-circularly polarized case ($\delta = -90$) for initial momenta $p_{1y} = p_{2y} = \pm 0.2mc$. Such symmetry is not seen. By symmetry we would expect the distributions in the case $p_{1z} = p_{2z}$ to be identical or qualitatively similar to the case $p_{1y} = p_{2y}$ since the initial momenta are in the transverse y-z plane with respect to the laser direction. However, this is not the case due to the interactions between helicity of the polarization and the electron spin along the z axis. The spin has no influence for the linearly polarized laser when the initial momenta are along the y or z direction. This observation shows there is interaction between the *helicity of circular polarization and the electron spin* when the initial electron moves along the spin axis, i.e., along z. This effect is the central result that emerges from systematic analysis of our computed results.

B. Superposed spins in the x-y momentum plane

Similar features are found in Fig. 8 when the distributions are viewed in the x-y momentum plane, but with stronger squeezing than in the y-z momentum plane. For initial momenta along the x direction, it is interesting that the squeezing is slightly greater for case $p_{1x} = p_{2x}$ with positive value than negative value, i.e., when both initial momenta of the spin-up electron move along the laser direction. This asymmetry shows the subtle *effect of the spin* direction. For initial momenta along the y direction and parallel, the distribution for positive value of $p_{1y} = p_{2y}$ is the *mirror image* of the distribution for negative value of $p_{1y} = p_{2y}$ upon reflection at $p_x = 0$. The distributions for initial momenta along the z direction (not shown) look quite identical to those for the x direction with unimportant differences. The distributions for the case of circular polarization are qualitatively the same as in the case of linear polarization except that the squeezing is stronger. This is because the the x-component squeezing is stronger than y-component squeezing by a factor $\frac{\xi}{|ea_y \cos\theta_j - \beta_{jy}\xi|}$ [according to Eq. (60)] that is greater than unity.

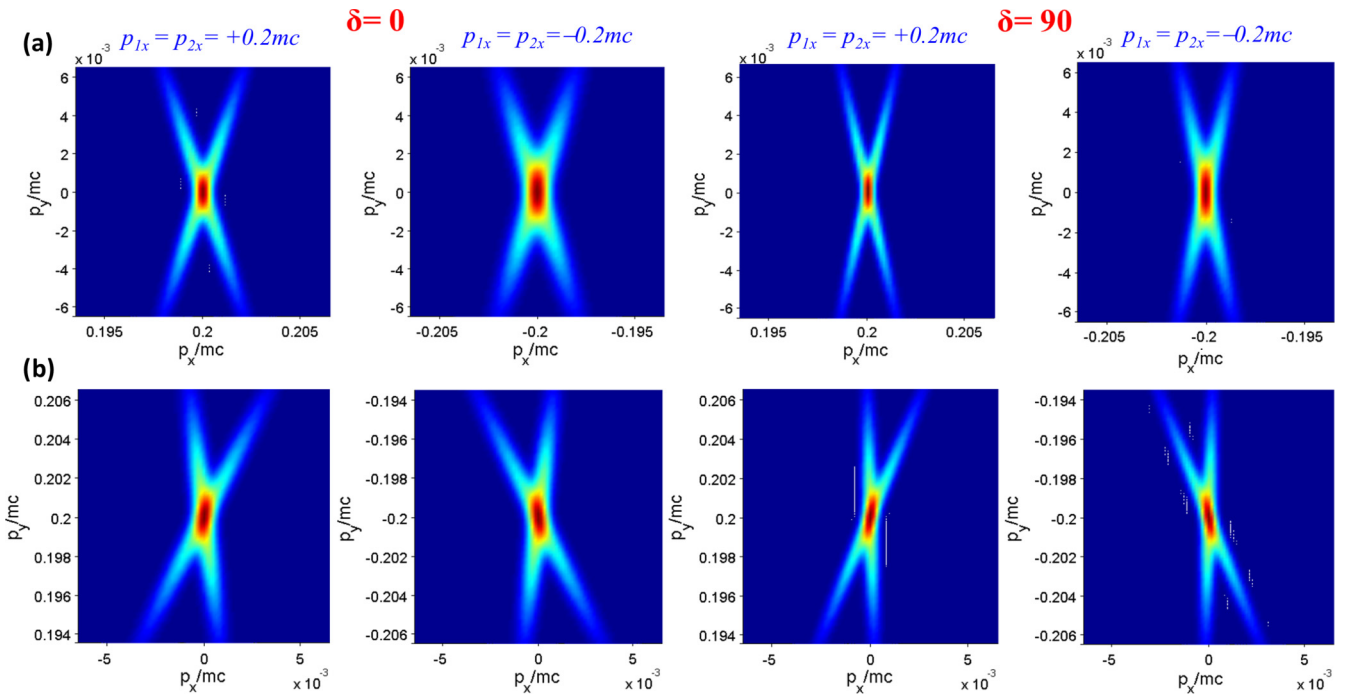

FIG. 8. Distributions $\Sigma_{s=1:4}|c^s(\mathbf{p})|^2$ on the x-y momentum plane at $p_z = p_{1z}$ for an electron in the superposed state driven by linearly polarized ($\delta = 0^\circ$) and circularly polarized ($\delta = 90^\circ$) lasers. Electron initial momenta along the (a) x direction and (b) y direction; plots for the z direction are not shown since the figures are quite similar to case (a), i.e., p_{jx}, p_{jy}, and p_{jz} (top to bottom panels). The initial momenta (left to right panels) are (i) $p_{1q} = p_{2q} = 0.2mc$ and (ii) $p_{1q} = p_{2q} = -0.2mc$ and $q = x, y, z$ for field $a\omega = 10^{15}$ V m^{-1}. (Cases for $p_{1q} = 0.2mc$, $p_{2q} = -0.2mc$ and $p_{1q} = -0.2mc$, $p_{2q} = 0.2mc$ have single squeezed distributions and are not shown.)

C. Two superposed states of the *same spin*

When the two electrons are spin up, an interference effect can be seen, as shown in Fig. 9 for the x-y plane and explained by Eq. (68). So, the interference feature enables the determination of the relative phase Φ by measuring the phase of the oscillations. However, no oscillations are seen in the y-z plane because it is transverse to the line joining the electron positions of the two states along the x axis, i.e., $-\hat{x}30d$ and $+\hat{x}30d$. On the other hand, if the superposed states are of opposite spins, but at the same initial position, say, at the origin, we also have interference in the distributions when the initial momenta have opposite directions.

Applying the solutions to the case of *two states with the same spin*, we may factor out the amplitude that contains the free-field solutions $u^s(\mathbf{p}, \mathbf{r}, t_0)$ which depend on all momentum components and also determine the momentum distribution but in a weaker manner than the exponential factors:

$$|c|^2 = K\left(\sum_{j=1,2}\Gamma_j^2 + \prod_{j=1:2}\Gamma_j 2\cos(\Omega_1 - \Omega_2 + \Phi)\right), \quad (68)$$

$$\Gamma_j = d_j^3\sqrt{\frac{E_j + mc^2}{2E_j}}e^{-(f_{4jy}^-{}^2 + f_{4jz}^-{}^2)d_j^2/2}e^{-G_j^2 d_j^2/2}, \quad (69)$$

$$\Omega_j = \varphi_j^- + f_{4jy}^- y_j + f_{4jz}^- z_j + \Xi(x_j) \quad (70)$$

with $K = \frac{N_0^2}{(2\pi)^4}\frac{E+mc^2}{2E}$. The second term has an important interference effect on the momentum distribution depicted in Fig. 9, which is what makes the distribution different from the simple algebraic sum.

VI. CONCLUSIONS AND OUTLOOK

In conclusion, the strong laser fields in the relativistic regime have significantly radical and interesting effects on the kinetics of electrons as shown through the momentum distributions. Numerical 3D plots provide bigger and insightful pictures on how the momentum distribution of relativistic electron scattering by intense laser fields is affected by the initial electron-spin direction, mean momentum, mean position, and quantum superposition as well as laser field strength, polarization, and phase. Using semianalytical solutions for arbitrary initial momentum at arbitrary position with generally elliptical polarization, we have systematically analyzed the effects of directionality of the initial mean momenta $\mathbf{p}_j$ and initial phase $\theta_j = \omega t_0 - k_x x_j$ on the symmetry of the momentum distributions for linear and circular polarizations.

In addition to providing clear and insightful explanation with analytical formulas to the momentum squeezing and rotations in the squeezed orientation we also discovered features in the momentum distributions such as bending or curvature of the squeezed distribution at sufficiently high intensity. The distortions occur because of relativistic effect due to nonlinear scattering of strong electromagnetic fields by the free moving relativistic electron even though the electron does not absorb any photon. The work done here, despite using a cw laser, provides a clean situation for clear and insightful understanding of the kinetic effects of strong laser fields on momentum of electrons in the relativistic regime. Further studies can be extended to atoms to better understand relativistic effects on momentum sharing [27], involve two laser beams with circular polarizations [28] and few cycle pulse envelopes, as

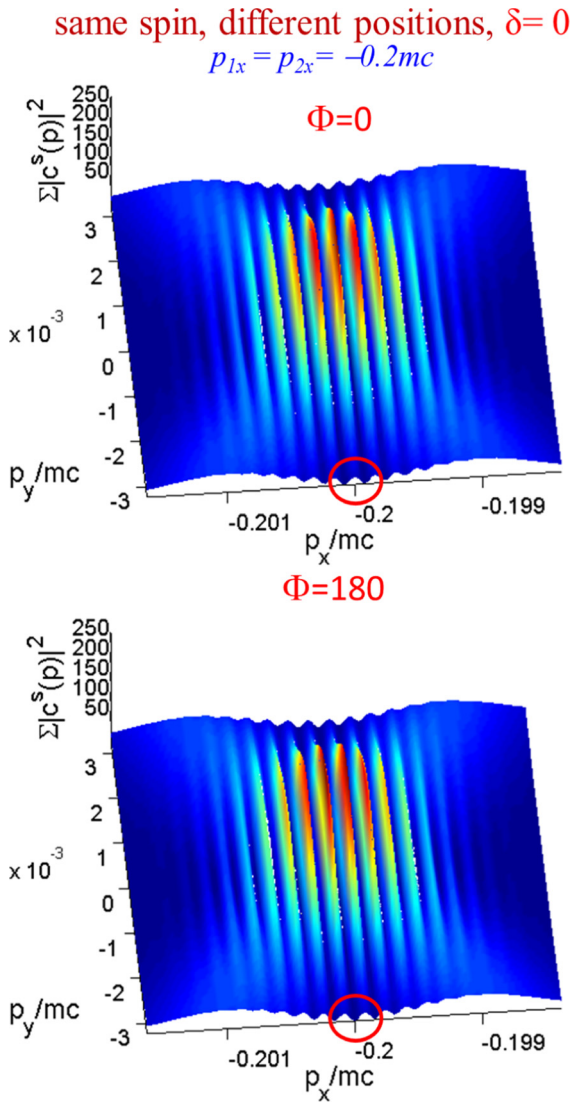

FIG. 9. Effects of the relative phase Φ between the two states on the distributions of the $\Sigma_{s=1:4}|c^s(\mathbf{p})|^2$ on the x-y momentum plane at $p_z = p_{1z}$ for two superposed states with the same spin (up) with linearly polarized laser ($\delta = 0^\circ$) and field strength $a\omega = 10^{15}$ V m^{-1}. The plots are for cases of electron initial momenta $p_{1q} = p_{2q} = -0.2mc$.

well as studies in strong magnetic fields and quantized laser fields [29,30].

APPENDIX A: SOLUTIONS OF THE COVARIANT DIRAC EQUATION

If we apply the operator $(\not{p} - e\not{A} + mc)$ to the left-hand side of each term of Eq. (1), we have the quadratic form of the Dirac equation:

$$\left[(\hat{p} - e\hat{A})^2 - \frac{1}{2}e\hbar\hat{\sigma}^{\mu\nu}F_{\mu\nu} - m^2c^2\right]\psi = 0, \tag{A1}$$

$$\hat{\sigma}^{\mu\nu}F_{\mu\nu} = 2i\not{k}\not{A}' = 2i\frac{1}{c}\alpha\cdot\mathbf{E} - 2\boldsymbol{\Sigma}\cdot\mathbf{B} \tag{A2}$$

where $\hat{p}$ is the operator of the canonical momentum. To make clear the adopted convention, we give explicitly the electromagnetic field tensor

$$F_{\mu\nu} = \partial_\mu A_\nu - \partial_\nu A_\mu = k_\mu A'_\nu - k_\nu A'_\mu \tag{A3}$$

$$= \begin{pmatrix} 0 & \frac{E_x}{c} & \frac{E_y}{c} & \frac{E_z}{c} \\ -\frac{E_x}{c} & 0 & -B_z & B_y \\ -\frac{E_y}{c} & B_z & 0 & -B_x \\ -\frac{E_z}{c} & -B_y & B_x & 0 \end{pmatrix} = \left[\frac{1}{c}\mathbf{E}, \mathbf{B}\right], \tag{A4}$$

and the antisymmetric tensor

$$\hat{\sigma}^{\mu\nu} = \frac{i}{2}[\gamma^\mu, \gamma^\nu] \tag{A5}$$

$$= \begin{pmatrix} 0 & i\alpha_1 & i\alpha_2 & i\alpha_3 \\ -i\alpha_1 & 0 & \Sigma_3 & -\Sigma_2 \\ -i\alpha_2 & -\Sigma_3 & 0 & \Sigma_1 \\ -i\alpha_3 & \Sigma_2 & -\Sigma_1 & 0 \end{pmatrix} = (i\alpha, -\boldsymbol{\Sigma}) \tag{A6}$$

with the matrices written as

$$\Sigma = \begin{pmatrix} \hat{\sigma} & \mathbf{0} \\ \mathbf{0} & \hat{\sigma} \end{pmatrix}, \quad \alpha = \gamma^0\gamma = \begin{pmatrix} \mathbf{0} & \hat{\sigma} \\ \hat{\sigma} & \mathbf{0} \end{pmatrix}, \tag{A7}$$

with $\Sigma_c = i\gamma^a\gamma^b$ where $a, b, c = x, y, z$ follow the cyclic permutations. The derivation of the solutions of the Dirac equation is given below.

Using $x_\mu = g_{\mu\nu}x^\nu$ or $\partial^\nu = g^{\nu\mu}\partial_\mu$ and the Lorentz gauge condition $\partial^\mu A_\mu = (\frac{\partial}{\partial ct}, -\nabla)\cdot(\frac{\phi}{c}, -\mathbf{A}) = \partial_\mu A^\mu = k_\mu A^{\mu\prime} = 0$ we have the relation

$$\hat{\sigma}^{\mu\nu}F_{\mu\nu} = i[\gamma^\mu\partial_\mu\gamma^\nu A_\nu + \gamma^\nu\partial_\nu\gamma^\mu A_\mu] = 2i\not{k}\not{A}' \tag{A8}$$

since $k\cdot A = 0$, $\gamma^\nu\gamma^0 = -\gamma^0\gamma^\nu$ for $\nu \neq 0$ where we use Lorentz gauge $\frac{1}{c^2}\frac{\partial\phi}{\partial t} + \nabla\cdot\mathbf{A} = \mathbf{0}$ and $\frac{\partial\mathbf{A}}{\partial t} + \nabla\phi = -\mathbf{E}$, and its Fourier transform $\frac{\omega}{c}\mathbf{A} + \frac{\phi}{c}\mathbf{k} \to \frac{\omega}{c}\mathbf{k}\cdot\mathbf{A} + \frac{\phi}{c}\mathbf{k}\cdot\mathbf{k} \to \mathbf{k}\cdot\mathbf{A} + \phi\frac{\omega}{c^2}$=0. Also, note that $(\gamma^{j=1,2,3})^2 = -I_4$ and $(\gamma\cdot\nabla)(\gamma\cdot\mathbf{A}) = -I_4\nabla\cdot\mathbf{A} - i\boldsymbol{\Sigma}\cdot\mathbf{B}$.

For positive (labeled superscript "+") and negative (labeled superscript "−") energies, replace the ansatz $\psi^\pm(\varphi) = e^{\mp ip\cdot x/\hbar}F^\pm(\varphi)u^\pm(\mathbf{p})$ into Eq. (A1):

$$[p^2 + e^2A^2 - e(A\cdot p) - e(p\cdot A) - ie\hbar\not{k}\not{A}' - m^2c^2]\psi^\pm(\varphi) = 0 \tag{A9}$$

where $\varphi = k\cdot x$, $u(\mathbf{p})$ is a four-component spinor, and p is a constant 4 vector with fixed modulus given by $p^2 = p^\mu p_\mu = (E/c)^2 - \mathbf{p}\cdot\mathbf{p} = m^2c^2$. Note that $\mathbf{p}$ is the quasicanonical momentum, from the ansatz, and it is not an eigenvalue of momentum operator $\hat{p}$.

We have the first-order linear differential equation

$$\left[2i\hbar k\cdot p\frac{\partial}{\partial\varphi} \pm e^2A^2 - 2e(A\cdot p) \mp i\hbar e\not{k}\not{A}'\right]F^\pm = 0 \tag{A10}$$

with the solution

$$F^\pm(\varphi) = \exp\left(-i\int_{-\infty}^{k\cdot x}V(\varphi)d\varphi\right)\exp\left(\pm\frac{e\not{k}\not{A}}{2(k\cdot p)}\right) \tag{A11}$$

where $V(\varphi) = [\frac{eA\cdot p}{\hbar(k\cdot p)} \mp \frac{e^2A^2}{2\hbar(k\cdot p)}]$, $p^2 - m^2c^2 = (E/c)^2 - |\mathbf{p}|^2 - m^2c^2 = 0$. Expansion of $\exp(\pm\frac{e\not{k}\not{A}}{2(k\cdot p)})$ gives

$$\psi^\pm = N(E)\left(1 \pm \frac{e\not{k}\not{A}}{2k\cdot p}\right)u^\pm(\mathbf{p})e^{iS^\pm} \tag{A12}$$

where

$$S^\pm = \mp\frac{p\cdot x}{\hbar} - \int_{-\infty}^{k\cdot x}\left[\frac{eA\cdot p}{\hbar(k\cdot p)} \mp \frac{e^2A^2}{2\hbar(k\cdot p)}\right]d\varphi \tag{A13}$$

with the normalization factor $N(E) = \sqrt{\frac{E+mc^2}{2E(2\pi)^3}}$. The solutions of the free-field Dirac equation are given in Appendix B.

APPENDIX B: SOLUTIONS OF THE FREE-FIELD DIRAC EQUATION

In the absence of vector and scalar potentials, the Dirac equation for spins with the quantization axis defined along the z direction (see Fig. 1) has the solutions

$$u^+ = \begin{pmatrix} \chi_s \\ \frac{c\hat{\sigma}\cdot\mathbf{p}}{E+mc^2}\chi_s \end{pmatrix}, \quad u^1 = \begin{pmatrix} 1 \\ 0 \\ \frac{p_z c}{E+mc^2} \\ \frac{(p_x+ip_y)c}{E+mc^2} \end{pmatrix},$$
$$u^2 = \begin{pmatrix} 0 \\ 1 \\ \frac{(p_x-ip_y)c}{E+mc^2} \\ \frac{-p_z c}{E+mc^2} \end{pmatrix}, \quad E > 0, \tag{B1}$$

$$u^- = \begin{pmatrix} \frac{c\hat{\sigma}\cdot\mathbf{p}}{|E|+mc^2}\chi_s \\ \chi_s \end{pmatrix}, \quad u^3 = \begin{pmatrix} \frac{p_z c}{|E|+mc^2} \\ \frac{(p_x+ip_y)c}{|E|+mc^2} \\ 1 \\ 0 \end{pmatrix},$$
$$u^4 = \begin{pmatrix} \frac{(p_x-ip_y)c}{|E|+mc^2} \\ \frac{-p_z c}{|E|+mc^2} \\ 0 \\ 1 \end{pmatrix}, \quad E < 0 \tag{B2}$$

where $p_\pm = p_x \pm ip_y$. Here, $u^s(\mathbf{p})$ are the free-particle Dirac solutions; $s = +$ represents 1 (spin up) and 2 (spin down) with positive energies, and $s = -$ represents 3 (spin up) or 4 (spin down) with negative energies. The spin vectors are $\chi_\uparrow = \binom{1}{0}$ and $\chi_\downarrow = \binom{0}{1}$, $s = \uparrow, \downarrow$.

APPENDIX C: ANALYSIS OF SPECIAL CASES

The following equations are helpful for analysis of the effects of different cases of initial momenta on the momentum squeezing in the figures:

$$\hbar G_j = \Delta p_{jx}\left(\frac{k_x\xi}{k\cdot p_j}(1-\beta_{jx}) - 1\right) + \Delta p_{jy}\frac{k_x}{k\cdot p_j}\{ea_y\cos\theta_j - \beta_{jy}\xi\} + \Delta p_{jz}\frac{k_x}{k\cdot p_j}\{ea_z\cos(\theta_j+\delta) - \beta_{jz}\xi\} \tag{C1}$$

$$= \Delta p_{jx}\left(\frac{k_x}{k\cdot p_j}\left\{e(\beta_{jy}A_y + \beta_{jz}A_z) - \frac{e^2|\mathbf{A}|^2}{2mc}\right\}(1-\beta_{jx}) - 1\right) + \tag{C2}$$
$$\frac{k_x}{(k\cdot p_j)}\left(\Delta p_{jy}\left\{\left(1-\beta_{jy}^2\right)eA_y - \beta_{jy}\beta_{jz}eA_z + \beta_{jy}\frac{e^2|\mathbf{A}|^2}{2mc}\right\} + \Delta p_{jz}\left\{-\beta_{jz}\beta_{jy}eA_y + \left(1-\beta_{jz}^2\right)eA_z + \beta_{jz}\frac{e^2|\mathbf{A}|^2}{2mc}\right\}\right).$$

where $\Delta p_{ju} = p_u - p_{ju}$, $\beta_{ju} = \frac{p_{ju}}{mc}$, $u = x, y, z$.

1. For $\mathbf{p}_j = \mathbf{0}$

$$\hbar G_j = -(p_x)\left(1 + \frac{k_x}{k\cdot p_j}\frac{e^2|\mathbf{A}(\theta_j)|^2}{2mc}\right) + \frac{k_x}{k\cdot p_j}[(p_y)ea_y\cos\theta_j + (p_z)ea_z\cos(\theta_j+\delta)]. \tag{C3}$$

2. For finite p_{jx}

$$\hbar G_j = -(p_x - p_{jx})\left(1 + \frac{k_x\left(1-\beta_{jx}^2\right)}{k\cdot p_j}\frac{e^2|\mathbf{A}(\theta_j)|^2}{2mc}\right) + \frac{k_x}{k\cdot p_j}e[p_y a_y\cos\theta_j + p_y a_z\cos(\theta_j+\delta)]. \tag{C4}$$

3. For finite p_{jy}

$$\hbar G_j = -p_x\left(1 - \frac{k_x\xi}{k\cdot p_j}\right) + \frac{k_x}{k\cdot p_j}[(p_y - p_{jy})\{ea_y\cos\theta_j - \beta_{jy}\xi\} + (p_z)ea_z\cos(\theta_j+\delta)] \tag{C5}$$

$$\xi \simeq e\beta_{jy}a_y\cos\theta_j - \frac{e^2|\mathbf{A}(\theta_j)|^2}{2mc}. \tag{C6}$$

4. For finite p_{jz}

$$\hbar G_j = -(p_x)\left(1 - \frac{k_x\xi}{k\cdot p_j}\right) + \frac{k_x}{k\cdot p_j}[(p_y)ea_y\cos\theta_j + (p_z - p_{jz})\{ea_z\cos(\theta_j+\delta) - \beta_{jz}\xi\}] \tag{C7}$$

$$\xi \simeq e\beta_{jz}a_z\cos(\theta_j+\delta) - \frac{e^2|\mathbf{A}(\theta_j)|^2}{2mc}. \tag{C8}$$

For finite p_{jz}, the distribution in the x-y plane generally depends on p_{jz} and becomes independent of p_{jz} only when $\theta_j + \delta = \pi/2$, because the term $ea_z \cos\delta$ would vanish.

[1] A. Di Piazza, Phys. Rev. Lett. **113**, 040402 (2014).

[2] C. Bula, K. T. McDonald, E. J. Prebys, C. Bamber, S. Boege, T. Kotseroglou, A. C. Melissinos, D. D. Meyerhofer, W. Ragg, D. L. Burke *et al.*, Phys. Rev. Lett. **76**, 3116 (1996); D. L. Burke, R. C. Field, G. Horton-Smith, J. E. Spencer, D. Walz, S. C. Berridge, W. M. Bugg, K. Shmakov, A. W. Weidemann, C. Bula *et al.*, **79**, 1626 (1997).

[3] D. M. Volkov, Z. Phys. **94**, 250 (1935).

[4] V. B. Berestetskii, E. M. Lifshitz, and L. P. Pitaevskii, *Quantum Electrodynamics* (Pergamon, New York, 1982).

[5] J. Bergou and S. Varro, J. Phys. A **13**, 2823 (1980).

[6] H. R. Reiss, J. Opt. Soc. Am. B **7**, 574 (1990).

[7] H. R. Reiss, Phys. Rev. A **42**, 1476 (1990).

[8] C. Yuce, Phys. Rev. A **74**, 062106 (2006).

[9] L. V. Keldysh, Zh. Eksp. Teor. Fiz. **47**, 1945 (1964) [Sov. Phys. JETP **20**, 1307 (1965)].

[10] H. R. Reiss and V. P. Krainov, Phys. Rev. A **50**, R910 (1994).

[11] J. Bauer, J. Phys. B **34**, 1343 (2001).

[12] F. V. Hartemann, S. N. Fochs, G. P. Le Sage, N. C. Luhmann, J. G. Woodworth, M. D. Perry, Y. J. Chen, and A. K. Kerman, Phys. Rev. E **51**, 4833 (1995).

[13] H. Prakash and N. Chandra, Nuovo Cimento B **55**, 404 (1968).

[14] A. Angioi, F. Mackenroth, and A. Di Piazza, Phys. Rev. A **93**, 052102 (2016).

[15] O. D. Skoromnik, I. D. Feranchuk, and C. H. Keitel, Phys. Rev. A **87**, 052107 (2013).

[16] S. Varro, Laser Phys. Lett. **10**, 095301 (2013).

[17] E. Raicher and S. Eliezer, Phys. Rev. A **88**, 022113 (2013).

[18] S. Chelkowski and A. D. Bandrauk, Mol. Phys. **115**, 1971 (2017).

[19] J. San Roman, L. Plaja, and L. Roso, Phys. Rev. A **64**, 063402 (2001).

[20] J. Peatross, C. Müller, and C. H. Keitel, Opt. Express **15**, 6053 (2007)

[21] J. San Roman, L. Roso, and H. R. Reiss, J. Phys. B **33**, 1869 (2000).

[22] V. P. Krainov, J. Phys. B **32**, 1607 (1999).

[23] N. Milosevic, P. B. Corkum, and T. Brabec, Phys. Rev. Lett. **92**, 013002 (2004).

[24] T. Zuo, A. D. Bandrauk, M. Ivanov, and P. B. Corkum, Phys. Rev. A **51**, 3991 (1995).

[25] D. B. Milošević and A. F. Starace, Phys. Rev. Lett. **82**, 2653 (1999).

[26] A. D. Bandrauk and H. Z. Lu, Phys. Rev. A **68**, 043408 (2003).

[27] S. Chelkowski, A. D. Bandrauk, and P. B. Corkum, Phys. Rev. Lett. **113**, 263005 (2014).

[28] M. Pardy, Int. J. Theor. Phys. **45**, 647 (2006).

[29] T. Alan and A. O. Barut, Europhys. Lett. **17**, 119 (1992).

[30] P. Filipowicz, J. Phys. A **18**, 1675 (1985).